Response to the comments for manuscript acp-2013-234

Title: A theoretical model on the formation mechanism and kinetics of highly toxic air pollutants from halogenated formaldehydes reacted with halogen atoms

Dear Prof. Rolf Sander and Prof. Natascha Töpfer,

We are sincerely grateful to your and the reviewer's attention on this paper. Please do forward our heartfelt thanks to the expert's critical comments and thoughtful suggestions. We have made careful modifications and revisions on the original manuscript according to the editor's and reviewers' comments. The changed sentences were marked as note in the PDF version, and you and the reviewers can be easily found these changes. Furthermore, we also send our paper out for English polishing to a professional language editing service before the submission. We hope that the revised paper will meet your standard. Below you will find our point-by-point responses to the reviewer's comments and questions:

Reviewer #2:

Question 1: *The manuscript should be carefully checked with respect to the use of English language. There are some grammatical errors in the paper, especially the usage of the article and plural.*

Response: We are very grateful to the reviewer's comments. We have already checked the English usage again and sent our paper out for English polishing to a professional language editing service before the submission.

Question 2: *The authors have compared two reaction mechanisms: hydrogen abstraction and X-addition. They should make it clear which mechanism is preferred for the reactions in the abstract.*

Response: According to the reviewer's helpful comments, the following sentence was corrected in the abstract as "Our studies showed that compared to X-addition pathway, the H-abstraction pathway was demonstrated to be more preferred to form halogenated formyl radicals and hydrogen halides. The radicals can be further degraded to CO_2, halogen molecules, and halogenated oxides." Because the X-addition pathways could be ignored and could not relevant to the atmospheric chemistry, the X-addition pathways were not discussed in the original manuscript.

Question 3: *I suggest the authors to change '3.2.1' section into '3.3' section.*

Response: According to the reviewer's useful comment, the '3.2.1' section was changed to '3.3' section in the revised version. The '3.2.1' section was the discussion of 'The fate of main atmospheric intermediates', and the '3.2' section was "kinetics" of X-initiated reaction. Therefore, it is necessary to change '3.2.1' section into '3.3' section.

Question 4: *In the last section, the authors analysed the effect of the altitude. In the supplement, the authors mentioned that the effect of the altitude is considered through the relationship between the altitude and the temperature. I suggest the authors to clarify such consideration in the manuscript. Since the calculated results are very important for their conclusions, could author move Table S10 into the paper*

Response: We are very thankful to the reviewer's helpful question**.** Table S10 was move to the main text as Table 4 according to the suggestion. In this work, the effect of the altitude was considered through the relationship between the altitude and the temperature. That is, in the troposphere, the temperature drops about 6.49 K for every 1 km increase in the altitude. Thus, in the stratosphere (from 11 km height above the earth surface), the constant temperature is kept at 216.69 K. Therefore, the relationship between the rate constant and the altitude can be easily obtained relative to the atmospheric temperature at the altitude.

Question 5: *In Table 1, ‘OH-addition pathway’ should be ‘X-addition pathway’.*

Response: According to the reviewer’s comment, the mistake was corrected in the Table 1.

Question 6: *In Fig. 2, the author should make it clear in the caption which reaction mechanism is used to calculate the relationship between the rate constants and 1000/T. And in the last image, kBr+BrCHO is missing.*

Response: We would like to thank the reviewer’s kind comment**.** Within the temperature range of 200–368 K, to obtain the beautiful and clear figure, the plot of the CVT/SCT rate constants versus 1000/T were obtained. According to the reviewer’s kind suggestion, for clarity, this caption and figure were improved more detail as follows:

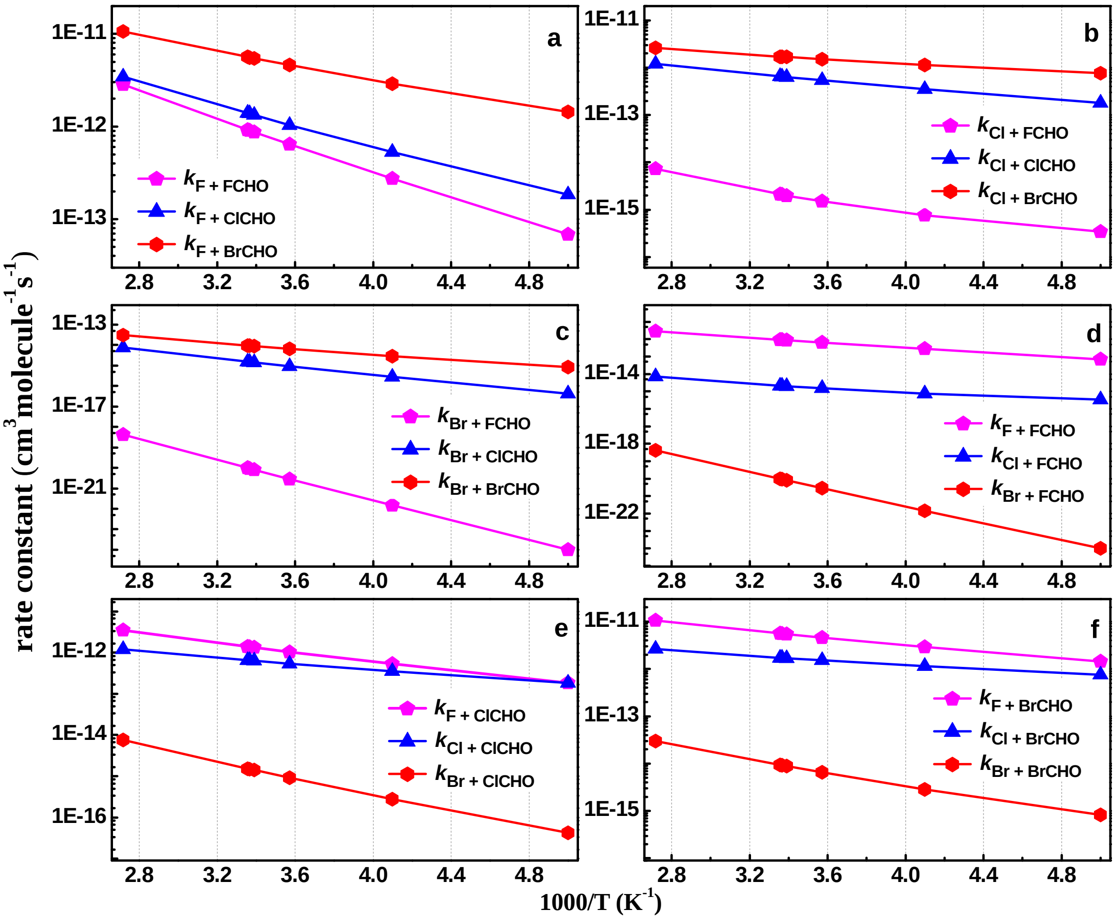

Fig. 2 Plot of the CVT/SCT rate constants versus 1000/T within the temperature range of 200–368 K for the reactions of (a) F + QCHO; (b) Cl + QCHO; (c) Br + QCHO; (d) X + FCHO; (e) X + ClCHO; (f) X + BrCHO. Here, X and Q = F, Cl, Br.

Question 7: *The caption 'Fig. 4' should be 'Scheme 1'.*

Response: We are very thankful to the reviewer's helpful question**.** Fig. 4 illustrates all the possible pathways for the title atmospheric reactions. Thus, according to the reviewer's kind suggestion, the "Fig. 4" was revised to "Scheme 1".

Atmos. Chem. Phys. Discuss., 13, 18205–18231, 2013
www.atmos-chem-phys-discuss.net/13/18205/2013/
doi:10.5194/acpd-13-18205-2013

Atmospheric
Chemistry
and Physics
Discussions
Open Access

A theoretical model on the formation mechanism and kinetics of highly toxic air pollutants from halogenated formaldehydes reacted with halogen atoms

Y. M. Ji[1], H. H. Wang[1,2], Y. P. Gao[1,2], G. Y. Li[1], and T. C. An[1]

[1]State Key Laboratory of Organic Geochemistry and Guangdong Key Laboratory of Environmental Resources Utilization and Protection, Guangzhou Institute of Geochemistry, Chinese Academy of Sciences, Guangzhou 510640, China
[2]Graduate School of Chinese Academy of Sciences, Beijing 100049, China

Received: 26 March 2013 – Accepted: 26 June 2013 – Published: 9 July 2013

Correspondence to: T. C. An (antc99@gig.ac.cn)

Published by Copernicus Publications on behalf of the European Geosciences Union.

Abstract

The atmospheric reactions of halogenated formaldehydes with halogen atoms were investigated by high-accuracy molecular orbital calculation. ~~Studie[illegible]owed that halogen atoms could easily abstract hydrogen atom from halogenated formaldehydes to form halogenated formyl radical and hydrogen halide (HX).~~ In specific areas with high concentration of halogen atoms, such as the marine boundary layer (MBL), halogenated formyl radical was easily to react with halogen atoms and finally transformed into HX and CO_2 in the presence of water; otherwise, this radical was degraded to CO_2, halogen gas, and halogenated oxide. By using the canonical variational transition state theory, the kinetics calculations were performed within a wide atmospheric temperature range of 200–368 K, and theoretical values agreed well with the available experimental data. Under atmospheric conditions, the rate constants decreased as altitude increased, and especially the rate constants of halogen atoms reaction with FCHO quickly reduced. Although the reactions of halogenated formaldehydes with F atoms were more easily occurred than did those with Cl and Br atoms, the two latter reactions were still important atmospheric degradation process, especially in the MBL. The modified Arrhenius formulas of rate constants within the atmospheric temperature range were fitted, which helped to understand the established atmospheric model and estimate the contribution of title reactions to atmospheric chemistry pollution.

1 Introduction

The Antarctic-like ozone hole was proposed in the Arctic in 2011 Nature paper (Manney et al., 2011). This proposal indicated that the implementation of the Montreal Protocol did not well restrain chlorofluorocarbons (CFCs) and hydrochlorofluorocarbons (HCFCs) to destroy the ozone and increase the stratospheric halogen loading (Manney et al., 2011; Newman et al., 2009) despite very low anthropogenic emission of CFCs, HCFCs and halogen (Manney et al., 1994; Newman et al., 2009). Halogenated formaldehydes are one of the halogenated molecules in the atmosphere, and they are reactive molecules to form the atmospheric degradation intermediates of several halocarbons such as CFCs and HCFCs (Hasson et al., 1998; Sanhueza et al., 1975; Wallington et al., 1992) as well as from the tropospheric reactions of halogen atoms with volatile organic compounds (VOCs) such as isoprene (Fantechi et al., 1998). On the other hand, the halogen species such as chlorine and bromine play an important role in the atmospheric chemical processes. Apart from anthropogenic organohalogen sources, another important sources is from sea-salt aerosols (Finlayson-Pitts, 2003) and the heterogeneous reactions on these aerosol surfaces (Rossi, 2003). Thus, high concentrations of these halogen species could be frequently found in the marine boundary layers (MBL) (Sommariva et al., 2012; Wingenter et al., 2005). Moreover, these halogen species are reactive toward various VOCs as well as ozone (Foster et al., 2001; Ofner et al., 2012; Riedel et al., 2012). Especially in occurrences of the depletion of surface ozone in the Atlantic and Arctic, the presence of high concentration of halogen atoms has been proven (Jobson et al., 1994; Read et al., 2008; Solberg et al., 1996). Thus, as a prelude to understand the role of VOCs in the atmospheric transformation, the atmospheric reactions of halogenated formaldehydes with halogen atoms are expected to be a significant process in some particular areas such as MBL.

So far, for the atmospheric reactions of three halogenated formaldehydes (FCHO, ClCHO and BrCHO) with three halogen atoms (F, Cl and Br), some of them have been investigated experimentally: FCHO + F (Behr et al., 1993, 1998; Francisco et al., 1990; Hasson et al., 1998; Meagher et al., 1997), FCHO + Cl (Bednarek et al., 1996; Edney et al., 1992; Meagher et al., 1997; Wallington et al., 1992), and ClCHO + Cl (Catoire et al., 1996; Libuda et al., 1990; Orlando, 1999; Sanhueza et al., 1975; Wallington et al., 1996). However, these experimental studies only focused on the kinetics data, and never involved in the reaction mechanisms. Nevertheless, to understand the transformation mechanisms and fate of atmospheric reaction intermediates (IM) is an indispensable component to assess the risk of various toxic VOCs (Blotevogel et al., 2010). As for the theoretical studies, only limited published data were reported on the reactions of FCHO + F (Francisco et al., 1990; Wu et al., 2003) and FCHO + Cl (Wu et al., 2002). And these studies achieved different conclusions regarding the contribution of addition pathways. For instance, the result obtained by Francisco et al. (Francisco et al., 1990) concluded that addition of fluorine atom onto FCHO was competitive, which contradicted Wu et al.'s results (Wu et al., 2003). Furthermore, no studies on the kinetic data of the addition pathways have been conducted by these theoretical researchers. To our knowledge, no experimental or theoretical investigations have been reported on the title reactions, except the ClCHO + Cl and FCHO + F/Cl reactions. Thus, to gain insight into the environmental impact of halogenated formaldehydes, a systematic theoretical study is required to illustrate the detailed atmospheric reaction mechanisms and kinetics of the title reactions, and the potential importance of the title reactions as an atmospheric degradation pathway is also deserved to qualitatively investigate with theoretical calculation method.

In this study, the atmospheric reaction mechanisms and kinetics of halogenated formaldehydes reaction with halogen atoms were investigated using the dual-level direct dynamics (DLD) method. The temperature-dependent rate constants of the title reactions in atmospheric environment were deduced using canonical variational transition state theory (CVT) with small curvature tunneling (SCT) to simulate the troposphere temperature range within the atmospheric temperature range of 200–368 K. Furthermore, the calculated data were compared with the available experimental results to assess the reliability of the proposed model.

2 Methods

All quantum chemistry and computational kinetics were calculated with Gaussian 03 program (Frisch et al., 2003) and Polyrate 9.4.1 program (Corchado et al., 2002), respectively. Geometric parameters and frequency calculations were carried out at the second-order Møller–Plesset perturbation theory (MP2) with sets of polarization function, i.e., MP2/6-311G(d,p). The vibrational frequencies were performed to characterize the nature of each point on the potential energy surface (PES) and make zero-point-energy (ZPE) corrections. Using the intrinsic reaction coordinate (IRC) theory, the minimum-energy path (MEP) was constructed to verify that each transition state (TS) uniquely connected the designated reactants with the products. The DLD method (Hu et al., 1996; Truhlar et al., 1996) was employed to investigate the reaction mechanisms and kinetics. The energy profiles of the title atmospheric reactions were refined at the PMP2/6-311+G(3df,3pd) level based on the geometries mentioned above. For simplicity, a double slash "//" was used to denote the dual-level dynamics approach such as PMP2//MP2. A higher energy calculation at quadratic configuration interaction with single, double and triple excitations [QCISD(T)] level was implemented to compare the performance of the PMP2 level for energies because the rate constants is sensitive to the energies. A full discussion was provided in Supplement (Table S1). The comparison showed that the PMP2//MP2 level of theory obtained a balance between accuracy and the computational cost. Based on the aforementioned results of quantum chemistry calculations, the products distributions and the rate constants of all the possible reaction pathways were computed using CVT (Truhlar et al., 1980) plus SCT (Liu et al., 1993).

3 Results and discussion

3.1 Atmospheric reaction mechanism

Generally, two different attack sites were present on the halogenated formaldehydes (QCHO, $Q = \text{F}$, Cl, and Br) by halogen atoms ($\text{X} = \text{F}$, Cl, and Br): the H atom was abstracted from the carbonyl group position (X-$\text{R}_{\text{abs-Q}}$) and the halogen atom was added onto the carbon atom of carbonyl group (X-$\text{R}_{\text{add-Q}}$) (Scheme 1). Figures S1 and S2 illustrated the geometries of reactants, products, TSs, and IMs calculated at the MP2/6-311G(d,p) level. To confirm the calculated geometry corresponding to a saddle point with only one imaginary frequency or a local minimum without imaginary frequency, the harmonic vibrational frequencies of the main stationary points were also listed in Table S2. The energy parameters were also presented in Table 1, including the reaction enthalpies (ΔH^0_{298}) and potential barrier heights (ΔE)obtained at the PMP2/6-311+G(3df,3pd)//MP2/6-311G(d,p) level. All geometries optimized at the MP2/6-311G(d,p) level and all energies obtained at the PMP2//MP2 level agreed with the available experimental data (Groner et al., 2001; Huisman et al., 1979; Nagai et al., 1981; NIST). The maximum relative errors were less than 0.01 % and 1.2 kcal mol^{-1} for the geometric parameters and energy parameters, respectively.

3.1.1 H-abstraction pathways

To compare the earliness of H-abstraction TS structures, a geometry parameter L was calculated using the variation in the breaking bond distance between TSs and reactants (δ(C–H)) as well as the forming bond distance between TSs and products (δ(H–X)): $L = \delta(\mathrm{C–H})/\delta(\mathrm{H}–X)$ (Table S3). This parameter L denoted not only a TS structure associated with a reactant-like or a product-like (L < 1 or L > 1) character, but also the quantification of the corresponding trend (Rayez et al., 1994). As shown in Table 1, except for Br-R$_{\text{abs-F}}$ and Br-R$_{\text{abs-Cl}}$ pathways (L > 1), all other pathways were exothermic reactions (L < 1); i.e., the reaction pathways with TS having a reactant-like character (L < 1) were exothermic reactions. Otherwise, it was expected to be endothermic. This conclusion was in accordance with the Hammond postulate (Hammond, 1955). In addition, a positive correlation was observed between L and ΔH^0_{298}; i.e, the lowest (highest) value of L corresponded to the lowest (highest) value of $\Delta \mathrm{H}^0_{298}$. For instance, the minimum (0.09) and maximum (3.25) L values of F-R$_{\text{abs-Br}}$ and Br-R$_{\text{abs-F}}$ pathways (Table S3) corresponded to the lowest and the highest ΔH^0_{298} with −56.04 kcal mol^{-1} and 11.34 kcal mol^{-1}, respectively (Table 1). For the attack of F atoms to three halogenated formaldehydes, the ΔEs of H-abstraction pathways were 1.29 kcal mol^{-1} for F-R$_{\text{abs-F}}$, −0.58 kcal mol^{-1} for F-R$_{\text{abs-Cl}}$, and −0.69 kcal mol^{-1} for F-R$_{\text{abs-Br}}$, respectively, decreasing with the order of ΔE(F-R$_{\text{abs-F}}$) > ΔE(F-R$_{\text{abs-Cl}}$) > ΔE(F-R$_{\text{abs-Br}}$). This result indicated that the H atom of halogenated formaldehydes should be abstracted more easily from FCHO to ClCHO to BrCHO. To further investigate the reactivity of H atom, the C–H bond-dissociation energies (D^0_{298}(C–H)) in carbonyl group were calculated, and the results were also listed in Table 1. For the three halogenated formaldehydes, the corresponding D^0_{298}(C–H) values were 96.42, 86.19, and 81.04 kcal mol^{-1}, respectively. This result was in line with the order of the ΔE, indicating that the halogen atom substitutions from F to Cl to Br atom can increase the reactivity of H atom. The reaction enthalpies obtained were −40.75 (F-R$_{\text{abs-F}}$), −50.89 (F-R$_{\text{abs-Cl}}$), and −56.04 (F-R$_{\text{abs-Br}}$) kcal mol^{-1}, exhibiting the same trend as that of potential barrier heights. Similar conclusions can be drawn regarding different halogenated formaldehydes reaction with Cl and Br atoms.

As for the attack of three halogen atoms to FCHO, the ΔEs and ΔH^0_{298}s were increased when the halogen atoms changed from F to Cl to Br atoms. This finding suggested that halogenated formaldehydes could be more easily abstracted by F atoms than Cl or Br atoms. However, some differences were observed in the reactions of ClCHO and BrCHO with different halogen atoms. The lowest ΔE was obtained in Cl-R$_{\text{abs-Cl}}$ (−1.25 kcal mol^{-1}) and Cl-R$_{\text{abs-Br}}$ (−1.56 kcal mol^{-1}) pathways (Table 1). For F-R$_{\text{abs-Cl}}$, Cl-R$_{\text{abs-Cl}}$, F-R$_{\text{abs-Br}}$, Cl-R$_{\text{abs-Br}}$, and Br-R$_{\text{abs-Br}}$ pathways, the energy barrier heights were positive without the ZPE corrections, while it became negative via the ZPE correction (Table 1). This result implied that all the aforementioned pathways can be nearly barrierless (see Supplement).

In addition, the standard formation enthalpy ($\Delta H^0_{f,298}$) of species is necessary to determine the kinetics of reaction process and the thermodynamic properties. Hence, the isodesmic reaction method (IUPAC) was performed to obtain the $\Delta H^0_{f,298}$ of main species without the experimental values, such as ClCHO, BrCHO, and the corresponding radicals, and are presented in Table S4. The method was used in this study as a hypothetical reaction, in which the chemical bond broken model in the reactants is the same as the formed model in the products. Therefore, the following isodesmic reactions were chosen due to the simple configuration of CH_4 (Ji et al., 2007):

$$QCHO + CH_4 \rightarrow HCHO + CH_3Q \quad (Q = F, Cl, Br) \qquad \text{(R1–R3)}$$

$$QCO + CH_4 \rightarrow HCO + CH_3Q \quad (Q = F, Cl, Br) \qquad \text{(R4–R6)}$$

The derivation procedure was as follows: (1) the SPE was calculated at the PMP2/6-311+G(3df,3pd) level using the geometries obtained by the MP2/6-311G(d,p) level for all products and reactants involved in Reactions (R1)–(R3) and Reactions (R4)–(R6). (2) The heat corrections were used to obtain the ΔH^0_{298} of Reactions (R1)–(R3) and Reactions (R4)–(R6) at 298 K using standard statistical thermodynamic methods. (3) The aforementioned reaction enthalpies were combined with the known experimental data in Reactions (R1)–(R3) and (R4)–(R6) (HCHO −27.69 kcal mol^{-1}; HCO −10.39 kcal mol^{-1}; CH_3Cl, −19.99 kcal mol^{-1}; CH_3F, −55.97 kcal mol^{-1}; CH_3Br, −9.08 kcal mol^{-1}; CH_4, −17.89 kcal mol^{-1}) (NIST) to calculate the required $\Delta H^0_{f,298}$. As shown in Table S4, the calculated $\Delta H^0_{f,298}$ were −46.55, −33.46, −6.10, and 1.78 kcal mol^{-1} for ClCHO, BrCHO, ClCO, and BrCO, respectively. Despite the lack of experimental data that prevents full comparison between the theoretical data and the experimental $\Delta H^0_{f,298}$, the calculated $\Delta H^0_{f,298}$ of FCHO (−93.53 kcal mol^{-1}) and FCO (−42.95 kcal mol^{-1}) were in line with the available experimental values (−89.96 kcal mol^{-1} and −41.95 kcal mol^{-1} for FCHO and FCO, respectively) in the reference (NIST). These results indicated that the PMP2//MP2 level can effectively model the $\Delta H^0_{f,298}$ of these species. Thus, it is expected that the calculated $\Delta H^0_{f,298}$ can provide reliable information for experimental investigations in the future.

3.1.2 X-addition pathways

For Cl or Br atoms addition to three halogenated formaldehydes, the ΔEs of these addition pathways were too high to overcome (Table 1), and these addition pathways were endothermic at least with 10 kcal mol^{-1} (ΔH^0_{298}). Thus, as indicated by the ΔE

and ΔH^0_{298}, the addition pathways mentioned above were not likely to occur under the atmospheric conditions. Therefore, this section will mainly focus on the pathways of F atoms addition onto three halogenated formaldehydes (F-addition pathway).

For the F-addition pathways (Fig. S2), the formation of C–F bond was always the same. Thus, the earliness of the TSs can be directly inferred from the forming C . . . F distance. That is, the longer the C . . . F distance is, the earlier the TS is (Iuga et al., 2008). Fig. S2 showed that the F-TS$_{\text{add-Cl}}$ pathway was the earliest among three addition TSs, suggesting that this pathway was more exothermic than the F-R$_{\text{add-F}}$ and F-R$_{\text{add-Br}}$ pathways according to the Hammond postulate (Hammond, 1955). From Table 1, the order of ΔH^0_{298}s were in line with that of TSs' geometrical feature mentioned above, and the ΔH^0_{298}s were −23.73 (F-R$_{\text{add-F}}$), −25.48 (F-R$_{\text{add-Cl}}$), and −23.02 (F-R$_{\text{add-Br}}$) kcal mol^{-1}, respectively. The ΔEs of F-R$_{\text{add-X}}$ pathways were 6.20, 7.57, and 8.23 kcal mol^{-1} (Table 1), respectively, with the increasing order of ΔE(F-R$_{\text{add-F}}$) < ΔE(F-R$_{\text{add-Cl}}$) < ΔE(F-R$_{\text{add-Br}}$). This result indicated that the addition pathways of F atom onto three halogenated formaldehydes would become increasingly more difficult as the molecular weight of halogen atom was increased in halogenated formaldehydes.

For the reaction of FCHO with F atoms, Francisco et al. asserted that the F-addition pathway should be competitive (Francisco et al., 1990); however, Wu et al. obtained a contrary conclusion (Wu et al., 2003). That is, this addition pathway can be completely disregarded. However, our calculation results mentioned above showed that the ΔE of F-addition pathway was higher than that of the corresponding H-abstraction pathway by only 4 kcal mol^{-1}, indicating a kinetic competition between the F-addition and H-abstraction pathways. On the other hand, the ΔH^0_{298} of F-addition pathway was higher than that of the H-abstraction pathways at least 17 kcal mol^{-1}, suggesting that the F-addition pathway can be ignored thermodynamically. The similar trend was observed for other title atmospheric reactions (F + ClCHO and F + BrCHO reactions). Thus, the contribution of the addition pathway cannot only be determined from the mechanism aspect but also from the kinetic aspect.

3.1.3 Natural bond orbital (NBO) calculation analysis

To further understand the nature of the title atmospheric reaction mechanisms, the distribution of molecular electrostatic potential as well as NBO charges were carried out at the MP2/6-311G(d,p) level. The results were illustrated in Fig. 1. The most positive and negative potential were assigned to be blue and red, respectively. The more positive potential bond (bluer) is preferred to the nucleophiles attack. Therefore, the blue color of H atoms was deeper than that of C atoms in three halogenated formaldehydes (Fig. 1). That is, the H atoms appeared to have stronger positive potential bond than the C atoms. This finding suggested that the H-abstraction pathways were expected to more likely occur than the corresponding X-addition pathways. The NBO charges estimated for H atoms were 0.105, 0.139, and 0.141 e, respectively, indicating an increased trend from FCHO to ClCHO to BrCHO. Therefore, the H atoms in three molecules were more and more easy to be abstracted by halogen atoms and could be explained in terms of the inductive effect of halogen substitution. For three halogenated formaldehydes, the inductive effect gradually weakens from the electron group -F to -Cl to -Br, and thus the lone pair of electrons on the C atom of carbonyl group were harder and harder to be attracted, thereby increasing the electron density of H atom. As expected, the reactivity of the H-abstraction pathway should be increased from FCHO to ClCHO and then to BrCHO.

3.2 Reaction kinetics

The theoretical predictions herein can help us to develop reliable models for the real atmospheric reactions occurring within the temperature range from the earth surface to tropopause (200–368 K). Therefore, in this section, the DLD calculations were performed with CVT plus interpolated single-point energies method (Chuang et al., 1999) using the PMP2//MP2 level to compute the rate constants at every 10 K as well as the temperature point with the experimental values. For the convenience of the following discussion, the calculated rate constants using CVT plus SCT were denoted as

CVT/SCT rate constants. The obtained rate constants and the available experimental data were compared in Fig. S3. The temperature dependences of branching ratios between the H-abstraction and the X-addition pathways were also exhibited in Fig. S4. Tables S5 to S7 list the rate constants of each pathway and the total rate constants.

The CVT/SCT rate constants of the F-$R_{abs\text{-}F}$ pathway (Fig. S3a) were in good agreement with most experimental data (Behr et al., 1993, 1998; Francisco et al., 1990; Hasson et al., 1998; Meagher et al., 1997). For example, the calculated rate constant of 9.26×10^{-13} cm^3 molecule^{-1} s^{-1} at 298 K perfectly matched with the experimental values of $(8.8 \pm 1.4) \times 10^{-13}$ cm^3 molecule^{-1} s^{-1} (Behr et al., 1993) and $(8.0 \pm 1.0) \times 10^{-13}$ cm^3 molecule^{-1} s^{-1} (Hasson et al., 1998), but was slightly lower than that of 2.11×10^{-12} cm^3 molecule^{-1} s^{-1} (Francisco et al., 1990). With respect to Cl-$R_{abs\text{-}F}$ pathway (Fig. S3b), the rate constants matched with the available experimental data (Bednarek et al., 1996; Edney et al., 1992; Meagher et al., 1997; Wallington et al., 1992) in the temperature range of 244–298 K due to the largest deviation within a factor of 1.6. For instance, the calculated rate constant of 1.99×10^{-15} cm^3 molecule^{-1} s^{-1} at 295 K agreed well with the experimental values of $(1.9 \pm 0.2) \times 10^{-15}$ (Meagher et al., 1997) and $(2.1 \pm 0.2) \times 10^{-15}$ cm^3 molecule^{-1} s^{-1} (Edney et al., 1992). For Cl-$R_{abs\text{-}Cl}$ pathway (Fig. S3c), the calculated rate constant was slightly lower than the data achieved by Sanhueza et al. at 305 K (Sanhueza et al., 1975), but were well accord with other experimental data (Catoire et al., 1996; Libuda et al., 1990; Orlando, 1999; Wallington et al., 1996). Fitted by the CVT/SCT rate constants, the Arrhenius expression was obtained to be $0.99 \times 10^{-11} \exp(-813/T)$ cm^3 molecule^{-1} s^{-1}, which was in agreement with the experimental expressions of $1.39 \times 10^{-11} \exp[(-866 \pm 168)/T]$ cm^3 molecule^{-1} s^{-1} within the temperature range 266–322 K (Libuda et al., 1990). On the basis of the previous discussion, the theoretical results matched well with the available experimental data owing to the largest deviation factor of 2.6. Thus, the rate constants obtained at the PMP2//MP2 levels were reliable within the atmospheric temperature range from 200 to 368 K, which is particularly important for the atmospheric reactions without experimental data.

The total rate constants of same halogen atom reaction with different halogenated formaldehydes within the temperature range of 200–368 K were demonstrated in Fig. 2a–c. These rate constants at 298 K were also presented in Table 2. For the reactions of F atom with different halogenated formaldehydes (Table 2), the total rate constants obtained were 9.26×10^{-13} (F + FCHO), 1.40×10^{-12} (F + ClCHO), and 5.64×10^{-12} (F + BrCHO) $\mathrm{cm^3\,molecule^{-1}\,s^{-1}}$ at 298 K. The rate constants increased in the order of $k(\mathrm{F + FCHO}) < k(\mathrm{F + ClCHO}) < k(\mathrm{F + BrCHO})$, which was consistent with the analysis values of potential barrier and NBO calculation. The similar results can be drawn from the reactions of different halogenated formaldehydes with Cl or Br atoms. For the same halogenated formaldehyde reactions with different halogen atoms, the total CVT/SCT results were also summarized in Fig. 2d–f. For the reactions of ClCHO with different halogen atoms (Fig. 2d), the theoretical results decreased in the order of $k(\mathrm{F + ClCHO}) > k(\mathrm{Cl + ClCHO}) > k(\mathrm{Br + ClCHO})$. The similar trend can also be observed for the reactions of FCHO and BrCHO with different halogen atoms. Although the results showed that the reactions of F atoms with halogenated formaldehydes were more important in the degradation processes than those with Cl and Br atoms, the halogenated formaldehydes reacted with Cl and Br atoms were still important under the atmospheric condition due to high concentration of Cl and Br atoms in the MBL. To confirm the contributions of halogen atoms in halogenated formaldehydes, the rate constants of parent formaldehyde reaction with halogen atoms reported by Beukes et al. (Beukes et al., 2000) were also presented in Table 2. The rate constants of formaldehydes with halogen atoms were larger than those of halogenated formaldehydes with the corresponding halogen atoms. This result indicated that the decrease in the atmospheric activities of three halogenated formaldehydes with halogen atom substitution compared with their parent formaldehydes.

Figure S4 showed that for all nine atmospheric reactions, the contribution of all X-addition pathways to the total rate constant was almost equal to zero. Such finding suggested that the addition–elimination pathways were negligible within the temperature range of 200–368 K. Therefore, the halogenated formyl radical (QCO, where Q = F, Cl, Br) and hydrogen halide (HX, where X = F, Cl, Br) were the dominant products, and the addition intermediates (such as $HC(O)F_2$, HC(O)ClF, etc.) were difficult to form at temperature range from 200 to 368 K.

To predict the rate constants of the title reactions in the temperatures without experimental data, the relationship was attempted between the temperature and the rate constants. Within the atmospheric temperature ranges of 200–368 K, the modified Arrhenius formulas were listed in Tables 3 and S8. The pre-exponential factor, the rate constants, and the activation energy can be drawn from these formulas.

~~3.2.1~~ The fate of main atmospheric intermediates

To better ascertain the environmental impact of the title atmospheric reactions, ClCO and HC(O)ClF were used as examples of the reaction intermediates of the H-abstraction and X-addition channels, respectively. The four possible atmospheric degradation pathways of ClCO radical were presented in Fig. 3, in which is corresponding to the elimination of Cl atom from ClCO (pathways 1), the reactions of ClCO with Cl atom (pathways 2 and 3) and oxygen atom (pathways 4). As shown in Fig. 3, the pathway 1 was difficult to occur because of higher potential barrier height than those of other pathways, whereas pathways 2–4 were all barrierless processes. To further confirm these barrierless processes, the point-wise potential curve was performed and the results were shown in Figs. S5–S7 (the detailed discussion is presented in Supplement). Pathways 2 and 3 were exothermic processes with the exothermic energies of –18.92 and –19.54 kcal mol^{-1} to form two isomers *cis*-$ClCO_3$ and *trans*-$ClCO_3$ with high activity, in which could be easily transformed to each other with a small internal rotation barrier (6.43 kcal mol^{-1}). Furthermore, both species can be easily degraded. For *trans*-$ClCO_3$, the most feasible pathway was to undergo a concerted O-shift and C–Cl bond cleavage, leading to the final products (CO_2 and ClO). Two *cis*-$ClCO_3$ could easily combine each other to produce CCl(O)OOCCl(O) owing to the low potential barrier heights with –19.91 kcal mol^{-1} and strongly exothermic energy with –35.37 kcal mol^{-1}. This intermediate CCl(O)OOCCl(O) could be further decomposed to produce CO_2 and Cl_2.

As for pathway 4, the ClCO radical could be prefer to react with Cl atom to form phosgene by a strong exothermic process with an energy decrease of −77.11 kcal mol^{-1}. Phosgene is well known to be slightly soluble in liquid water, in which it may yield CO_2 and HC1 as final gaseous products (Hatakeyama et al., 1989). Based on the aforementioned results, the ClCO radical could primarily react with Cl atoms to produce phosgene under high atmospheric concentration Cl atoms. Otherwise, the ClCO radical could be transformed into CO_2, Cl_2, and ClO by oxygen.

For the addition intermediate HC(O)ClF, there maybe exist three degradation pathways: H-elimination, Cl-elimination, and HF-elimination pathways (Scheme S1, as denoted F-$R_{\text{elm-Cl}}$1, F-$R_{\text{elm-Cl}}$2, and F-$R_{\text{elm-Cl}}$3). Table S9 listed the energies at different pathways, in which the energy of the corresponding intermediate was set to zero as reference. As shown in table, the ΔE of F-$R_{\text{elm-Cl}}$2 pathway was much lower at least 10 kcal mol^{-1} than those of F-$R_{\text{elm-Cl}}$1 and F-$R_{\text{elm-Cl}}$3 pathways. This result suggested that F-$R_{\text{elm-Cl}}$2 pathway could easily occur from the viewpoint of kinetics to release Cl atoms. However, the exothermic energy of the F-$R_{\text{elm-Cl}}$3 pathway (−33.17 kcal mol^{-1}) was lower 16 kcal mol^{-1} than that of the F-$R_{\text{elm-Cl}}$2 pathway. This indicated that the formation of HF and ClCO was thermodynamically favorable. Anyway, the addition pathways were difficult to occur, thus these products were not obtained under the atmospheric conditions.

~~3.5~~ Environmental implications

To evaluate the specific atmospheric region where the reactions of the halogenated formaldehydes with halogen atoms occur, the rate constants at different altitudes were also calculated (~~Table S10~~). From table, the rate constants decreased with increasing the altitudes, and the decrease in the halogen atom reaction with FCHO was faster than those of halogen atoms with other halogenated formaldehydes. For example, the rate constants at sea level were seven (F + FCHO), five (F + ClCHO), and three (F + BrCHO) times larger than those at 12 km height above sea level. As the results displayed in ~~Table S10~~ and Fig. S4, the QCO and HX were always found as dominated intermediates within the altitude between 0 and 12 km, but the products of addition pathways were difficult to produce. Particularly at sea level, the reaction intermediates of QCO and HX were obtained almost exclusively with the ratio of 100 %. According to previously mentioned results, the intermediate, QCO, was willing to react with halogen atoms to form unstable compounds in specific areas with high concentrations of halogen atoms (for example, MBL). These compounds were slightly soluble and then yield CO_2 and HX as final gaseous products. Otherwise, the QCO were degraded to form CO_2, X_2, and XO. In particular, for the reaction of ClCHO with Cl atoms, the phosgene and ClO were found during the atmospheric degradation process. Phosgene is well known as a highly toxic colorless gas (Fu et al., 2007) that can endanger human health via inhalation and exposure (Stanek et al., 2011), and ClO is also a key ozone destruction catalyst (Solomon, 1999). Therefore, halogenated formaldehydes as intermediates of the atmospheric degradation of VOCs, need an ongoing comprehensive attention and further risk assessment in atmospheric environment.

Supplement

(1) Detailed descriptions of the computational methods and comparison of methods; (2) details on frequencies for species, parameters of energies, and ratios; (3) detailed comparison between the theoretical and the experimental values; and (4) CVT/SCT rate constants and Arrhenius formulas for each pathway within the temperature range of 200–368 K. These materials are available free of charge via the internet at http://www.atmospheric-chemistry-and-physics.net/home.html.

Supplementary material related to this article is available online at: http://www.atmos-chem-phys-discuss.net/13/18205/2013/acpd-13-18205-2013-supplement.pdf.

Acknowledgements. This is contribution No. IS-1606 from GIGCAS. This work was financially supported by the Team Project from Natural Science Foundation of Guangdong Province, China (S2012030006604), the National Natural Science Foundation of China (41205088) and the Science and Technology Project of Guangdong Province, China (2011A030700003 and 2012A032300017). We also thank Professor Donald G. Truhlar for his providing POLYRATE program.

References

Bednarek, G., Breil, M., Hoffmann, A., Kohlmann, J. P., Mors, V., and Zellner, R.: Rate and mechanism of the atmospheric degradation of 1,1,1,2-tetrafluoroethane (HFC-134a), Ber. Bunsen Phys. Chem., 100, 528–539, 1996.

Behr, P., Goldbach, K., and Heydtmann, H.: The reaction of fuorine atoms with formyl fluoride and the CFO self-reaction at 293 K, Int. J. Chem. Kinet., 25, 957–967, 1993.

Behr, P., Kaupert, C., Shafranovski, E., and Heydtmann, H.: Temperature dependence of the gas-phase reactions F + CHFO, CFO + F, and CFO + CFO, Int. J. Chem. Kinet., 30, 329–333, 1998.

Beukes, J. A., D'Anna, B., Bakken, V., and Nielsen, C. J.: Experimental and theoretical study of the F, Cl and Br reactions with formaldehyde and acetaldehyde, Phys. Chem. Chem. Phys., 2, 4049–4060, 2000.

Blotevogel, J., Borch, T., Desyaterik, Y., Mayeno, A. N., and Sale, T. C.: Quantum chemical prediction of redox reactivity and degradation pathways for aqueous phase contaminants: an example with HMPA, Environ. Sci. Technol., 44, 5868–5874, 2010.

Catoire, V., Lesclaux, R., Schneider, W. F., and Wallington, T. J.: Kinetics and mechanisms of the self-reactions of CCl_3O_2 and $CHCl_2O_2$ radicals and their reactions with HO_2, J. Phys. Chem., 100, 14356–14371, 1996.

Chuang, Y. Y., Corchado, J. C., and Truhlar, D. G.: Mapped interpolation scheme for single-point energy corrections in reaction rate calculations and a critical evaluation of dual-level reaction path dynamics methods, J. Phys. Chem. A, 103, 1140–1149, 1999.

Corchado, J. C., Chang, Y. Y., Fast, P. L., Villa, J., Hu, W.-P., Liu, Y.-P., Lynch, G. C., Nguyen, K. A., Jackels, C. F., Melissas, V. S., Lynch, B. J., Rossi, I., Coitino, E. L., Fernandez-

Ramos, A., Pu, J. Z., Albu, T. V., Steckler, R., Garrett, B. C., Isaacson, A. D., and Truhlar, D. G.: POLYRATE version 9.4.1, University of Minnesota, Minneapolis, 2002.

Edney, E. O. and Driscoll, D. J.: Chlorine initiated photooxidation studies of hydrochlorofluorocarbons (HCFCs) and hydrofluorocarbons (HFCs): results for HCFC-22 ($CHClF_2$); HFC-41 (CH_3F); HCFC-124 ($CClFHCF_3$); HFC-125 (CF_3CHF_2); HFC-134a (CF_3CH_2F); HCFC-142b ($CClF_2CH_3$); and HFC-152a (CHF_2CH_3), Int. J. Chem. Kinet., 24, 1067–1081, 1992.

Fantechi, G., Jensen, N. R., Saastad, O., Hjorth, J., and Peeters, J.: Reactions of Cl atoms with selected VOCs: kinetics, products and mechanisms, J. Atmos. Chem., 31, 247–267, 1998.

Finlayson-Pitts, B. J.: The tropospheric chemistry of sea salt: a molecular-level view of the chemistry of NaCl and NaBr, Chem. Rev., 103, 4801–4822, 2003.

Foster, K. L., Plastridge, R. A., Bottenheim, J. W., Shepson, P. B., Finlayson-Pitts, B. J., and Spicer, C. W.: The role of Br_2 and BrCl in surface ozone destruction at polar sunrise, Science, 291, 471–474, 2001.

Francisco, J. S. and Zhao, Y.: The reaction of atomic fluorine with formyl fluoride: an experimental and theoretical study, J. Chem. Phys., 93, 276–286, 1990.

Frisch, M. J., Truck, G. W., Schlegel, H. B., Scuseria, G. E., Robb, M. A., Cheeseman, J. R., Zakrzewski, V. G., Montgomery, J. A., Stratmann, J. R. E., Burant, J. C., Dapprich, S., Millam, J. M., Daniels, A. D., Kudin, K. N., Strain, M. C., Farkas, O., Tomasi, J., Barone, V., Cossi, M., Cammi, R., Mennucci, B., Pomelli, C., Adamo, C., Clifford, S., Ochterski, J., Petersson, G. A., Ayala, P. Y., Cui, Q., Morokuma, K., Malick, D. K., Rabuck, A. D., Raghavachari, K., Foresman, J. B., Cioslowski, J., Ortiz, J. V., Boboul, A. G., Stefnov, B. B., Liu, G., Liaschenko, A., Piskorz, P., Komaromi, L., Gomperts, R., Martin, R. L., Fox, D. J., Keith, T., Al-Laham, M. A., Peng, C. Y., Nanayakkara, A., Gonzalez, C., Challacombe, M., Gill, P. M. W., Johnson, B., Chen, W., Wong, M. W., Andres, J. L., Gonzalez, C., Head-Gordon, M., Replogle, E. S., and Pople, J. A.: Revision A.1, GAUSSIAN 03, Guassian, Inc., Pittsburgh, PA, 2003.

Fu, D. J., Boone, C. D., Bernath, P. F., Walker, K. A., Nassar, R., Manney, G. L., and McLeod, S. D.: Global phosgene observations from the Atmospheric Chemistry Experiment (ACE) mission, Geophys. Res. Lett., 34, L17815, doi:10.1029/2007GL029942, 2007.

Groner, P. and Warren, R. D.: Approximate r(e) structures from experimental rotational constants and ab initio force fields, J. Mol. Struct., 599, 323–335, 2001.

Hammond, G. S.: A correlation of reaction rates, J. Am. Chem. Soc., 77, 334–338, 1955.

Hasson, A. S., Moore, C. M., and Smith, I. W. M.: The fluorine atom initiated oxidation of CF_3CFH_2 (HFC-134a) studied by FTIR spectroscopy, Int. J. Chem. Kinet., 30, 541–554, 1998.

Hatakeyama, S. and Leu, M. T.: Rate constants for reactions between atmospheric reservoir species, 2. H_2O, J. Phys. Chem., 93, 5784–5789, 1989.

Hu, W. P. and Truhlar, D. G.: Factors affecting competitive ion-molecule reactions: $ClO^-+C_2H_5Cl$ and C_2D_5Cl via E2 and S_N2 channels, J. Am. Chem. Soc., 118, 860–869, 1996.

Huisman, P. A. G., Klebe, K. J., Mijlhoff, F. C., and Renes, G. H.: Molecular-structure of formyl fluoride in the gas-phase as determined from electron-diffraction and microwave data, J. Mol. Struct., 57, 71–82, 1979.

Iuga, C., Galano, A., and Vivier-Bunge, A.: Theoretical investigation of the OH-initiated oxidation of benzaldehyde in the troposphere, ChemPhysChem, 9, 1453–1459, 2008.

IUPAC: available at: http://goldbook.iupac.org/I03272.html, last access: March 2013.

Ji, Y. M., Zhao, X. L., Li, Z. S., and Liu, J. Y.: Kinetic mechanism of the hydrogen abstraction reactions of the chlorine atoms with CH_3CF_2Cl and CH_3CFCl_2: a dual level direct dynamics study, J. Comput. Chem., 28, 975–983, 2007.

Jobson, B. T., Niki, H., Yokouchi, Y., Bottenheim, J., Hopper, F., and Leaitch, R.: Measurements of C2-C6 hydrocarbons during the polar sunrise 1992 experiment – evidence for Cl atom and Br atom chemistry, J. Geophys. Res.-Atmos., 99, 25355–25368, 1994.

Libuda, H. G., Zabel, F., Fink, E. H., and Becker, K. H.: Formyl chloride: UV absorption cross sections and rate constants for the reactions with Cl and OH, J. Phys. Chem., 94, 5860–5865, 1990.

Liu, Y. P., Lu, D. H., Gonzalezlafont, A., Truhlar, D. G., and Garrett, B. C.: Direct dynamics calculation of the kinetic isotope effect for an organic hydrogen-transfer reaction, including corner-cutting tunneling in 21 Dimensions, J. Am. Chem. Soc., 115, 7806–7817, 1993.

Manney, G. L., Froidevaux, L., Waters, J. W., Zurek, R. W., Read, W. G., Elson, L. S., Kumer, J. B., Mergenthaler, J. L., Roche, A. E., Oneill, A., Harwood, R. S., Mackenzie, I., and Swinbank, R.: Chemical depletion of ozone in the arctic – lower stratosphere during winter 1992–93, Nature, 370, 429–434, 1994.

Manney, G. L., Santee, M. L., Rex, M., Livesey, N. J., Pitts, M. C., Veefkind, P., Nash, E. R., Wohltmann, I., Lehmann, R., Froidevaux, L., Poole, L. R., Schoeberl, M. R., Haffner, D. P., Davies, J., Dorokhov, V., Gernandt, H., Johnson, B., Kivi, R., Kyro, E., Larsen, N., Levelt, P. F., Makshtas, A., McElroy, C. T., Nakajima, H., Parrondo, M. C., Tarasick, D. W., von der Gathen, P., Walker, K. A., and Zinoviev, N. S.: Unprecedented arctic ozone loss in 2011, Nature, 478, 469–465, 2011.

Meagher, R. J., McIntosh, M. E., Hurley, M. D., and Wallington, T. J.: A kinetic study of the reaction of chlorine and fluorine atoms with HC(O)F at 295 ± 2 K, Int. J. Chem. Kinet., 29, 619–625, 1997.

Nagai, K., Yamada, C., Endo, Y., and Hirota, E.: Infrared diode-laser spectroscopy of FCO- the NU-1 and NU-2 bands, J. Mol. Spectrosc., 90, 249–272, 1981.

Newman, P. A., Oman, L. D., Douglass, A. R., Fleming, E. L., Frith, S. M., Hurwitz, M. M., Kawa, S. R., Jackman, C. H., Krotkov, N. A., Nash, E. R., Nielsen, J. E., Pawson, S., Stolarski, R. S., and Velders, G. J. M.: What would have happened to the ozone layer if chlorofluorocarbons (CFCs) had not been regulated?, Atmos. Chem. Phys., 9, 2113–2128, doi:10.5194/acp-9-2113-2009, 2009.

NIST: available at: http://webbook.nist.gov/chemistry/, last access: March 2013.

Ofner, J., Balzer, N., Buxmann, J., Grothe, H., Schmitt-Kopplin, Ph., Platt, U., and Zetzsch, C.: Halogenation processes of secondary organic aerosol and implications on halogen release mechanisms, Atmos. Chem. Phys., 12, 5787–5806, doi:10.5194/acp-12-5787-2012, 2012.

Orlando, J. J.: Temperature dependence of the rate coefficients for the reaction of chlorine atoms with chloromethanes, Int. J. Chem. Kinet., 31, 515–524, 1999.

Rayez, M. T., Rayez, J. C., and Sawerysyn, J. P.: Ab-Initio Studies of the reactions of chlorine atoms with fluorosubstituted and chlorosubstituted methanes, J. Phys. Chem., 98, 11342–11352, 1994.

Read, K. A., Mahajan, A. S., Carpenter, L. J., Evans, M. J., Faria, B. V. E., Heard, D. E., Hopkins, J. R., Lee, J. D., Moller, S. J., Lewis, A. C., Mendes, L., McQuaid, J. B., Oetjen, H., Saiz-Lopez, A., Pilling, M. J., and Plane, J. M. C.: Extensive halogen-mediated ozone destruction over the tropical Atlantic Ocean, Nature, 453, 1232–1235, 2008.

Riedel, T. P., Bertram, T. H., Crisp, T. A., Williams, E. J., Lerner, B. M., Vlasenko, A., Li, S. M., Gilman, J., de Gouw, J., Bon, D. M., Wagner, N. L., Brown, S. S., and Thornton, J. A.: Nitryl chloride and molecular chlorine in the coastal marine boundary layer, Environ. Sci. Technol., 46, 10463–10470, 2012.

Rossi, M. J.: Heterogeneous reactions on salts, Chem. Rev., 103, 4823–4882, 2003.

Sanhueza, E. and Heicklen, J.: Chlorine-atom sensitized oxidation of dichloromethane and chloromethane, J. Phys. Chem., 79, 7–11, 1975.

Solberg, S., Schmidbauer, N., Semb, A., Stordal, F., and Hov, O.: Boundary-layer ozone depletion as seen in the Norwegian Arctic in Spring, J. Atmos. Chem., 23, 301–332, 1996.

Solomon, S.: Stratospheric ozone depletion: a review of concepts and history, Rev. Geophys., 37, 275–316, 1999.

Sommariva, R., and von Glasow, R.: Multiphase halogen chemistry in the tropical Atlantic Ocean, Environ. Sci. Technol., 46, 10429–10437, 2012.

Stanek, L. W., Brown, J. S., Stanek, J., Gift, J., and Costa, D. L.: Air pollution toxicology – a brief review of the role of the science in shaping the current understanding of air pollution health risks, Toxicol. Sci., 120, S8–S27, 2011.

Truhlar, D. G. and Garrett, B. C.: Variational transition-state theory, Acc. Chem. Res., 13, 440–448, 1980.

Truhlar, D. G., Garrett, B. C., and Klippenstein, S. J.: Current status of transition-state theory, J. Phys. Chem., 100, 12771–12800, 1996.

Wallington, T. J., Hurley, M. D., Ball, J. C., and Kaiser, E. W.: Atmospheric chemistry of hydrofluorocarbon 134a: Fate of the alkoxy radical CF_3CFHO, Environ. Sci. Technol., 26, 1318–1324, 1992.

Wallington, T. J., Hurley, M. D., and Schneider, W. F.: Atmospheric chemistry of CH_3Cl: mechanistic study of the reaction of CH_2ClO_2 radicals with HO_2, Chem. Phys. Lett., 251, 164–173, 1996.

Wingenter, O. W., Sive, B. C., Blake, N. J., Blake, D. R., and Rowland, F. S.: Atomic chlorine concentrations derived from ethane and hydroxyl measurements over the equatorial Pacific Ocean: implication for dimethyl sulfide and bromine monoxide, J. Geophys. Res.-Atmos., 110, D20308, doi:10.1029/2005JD005875, 2005.

Wu, H. Y., Liu, J. Y., Li, Z. S., Huang, X. R., and Sun, C. C.: Theoretical study and rate constant calculation for the F + CHFO reaction, Chem. Phys. Lett., 369, 504–512, 2003.

Wu, J. Y., Liu, J. Y., Li, Z. S., Huang, X. R., and Sun, C. C.: Direct ab initio dynamics calculations of the reaction rates for the hydrogen abstraction reaction Cl + HC(O)F > HCl + CFO, Phys. Chem. Chem. Phys., 4, 2927–2931, 2002.

Table 1. Energy parameters, including the potential barrier heights (ΔE), reaction enthalpies (ΔH^0_{298}), and dissociation energies [D^0_{298}(C–H)] for the title reactions QCHO + X → products (in kcal mol^{-1}).

QCHO \ X	F		Cl		Br		D^0_{298}(C–H)
	ΔE	ΔH^0_{298}	ΔE	ΔH^0_{298}	ΔE	ΔH^0_{298}	
H-abstraction pathways							
FCHO	1.29	−40.75[a](−35.14)	2.64	−3.36[a](−2.15)	11.34	10.26 [a](13.63)	96.42
ClCHO	−0.58	−50.89	−1.25	−14.13	5.69	0.07	86.19
BrCHO	−0.69	−56.04	−1.56	−18.63	−0.53	−5.07	81.04
~~OH addition~~ pathways							
FCHO	6.20	−23.73	16.14	15.17	23.12	25.88	
ClCHO	7.57	−25.48	15.24	20.49	20.54	23.93	
BrCHO	8.23	−23.02	15.14	10.05	20.12	56.68	

[a] Experimental value (NIST).

Table 2. Total rate constants of the X + QCHO reactions at 298 K (in $\mathrm{cm^3\,molecule^{-1}\,s^{-1}}$).

QCHO \ X	F	Cl	Br
	$k_{\mathrm{CVT/SCT}}$	$k_{\mathrm{CVT/SCT}}$	$k_{\mathrm{CVT/SCT}}$
FCHO	9.26×10^{-13}	2.11×10^{-15}	9.87×10^{-21}
ClCHO	1.40×10^{-12}	6.52×10^{-12}	1.53×10^{-15}
BrCHO	5.64×10^{-12}	1.71×10^{-12}	9.41×10^{-15}
HCHO[a]	4.5×10^{-11}	8.0×10^{-11}	1.8×10^{-12}

[a] From the experimental data (Beukes et al., 2000).

Table 3. The modified Arrhenius formulas for $k = AT^B \exp(-C/T)$ within the temperature range of 200–368 K.

Reaction	A^a	B	C^b
$FCHO + F \rightarrow$ products	4.39×10^{-16}	1.99	1102
$ClCHO + F \rightarrow$ products	4.48×10^{-17}	2.22	694
$BrCHO + F \rightarrow$ products	3.71×10^{-16}	1.91	374
$FCHO + Cl \rightarrow$ products	1.80×10^{-41}	9.78	−1275
$ClCHO + Cl \rightarrow$ products	5.39×10^{-18}	2.20	243
$BrCHO + Cl \rightarrow$ products	3.50×10^{-17}	1.91	31
$FCHO + Br \rightarrow$ products	4.21×10^{-21}	3.02	4866
$ClCHO + Br \rightarrow$ products	1.53×10^{-23}	3.96	1228
$BrCHO + Br \rightarrow$ products	5.41×10^{-24}	4.03	501

[a] Units in cm^3 $molecule^{-1}$ s^{-1}.

[b] $B = \frac{E}{R}$, $E = E_a - nRT$, R is the gas constant (Zheng et al., 2010).

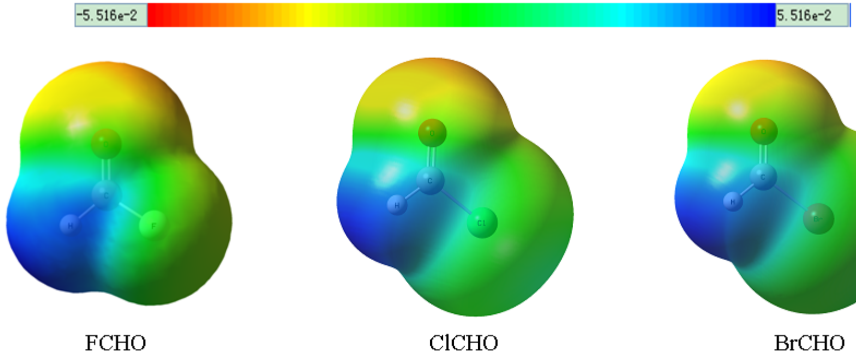

Atom	NBO charges
C	0.924
H	0.105
O	-0.614
F	-0.414

Atom	NBO charges
C	0.530
H	0.139
O	-0.578
Cl	-0.091

Atom	NBO charges
C	0.491
H	0.141
O	-0.575
Br	-0.058

Fig. 1. Calculated molecular electrostatic potential and NBO charges (in e) for the reactants at the MP2/6-311G(d,p) level.

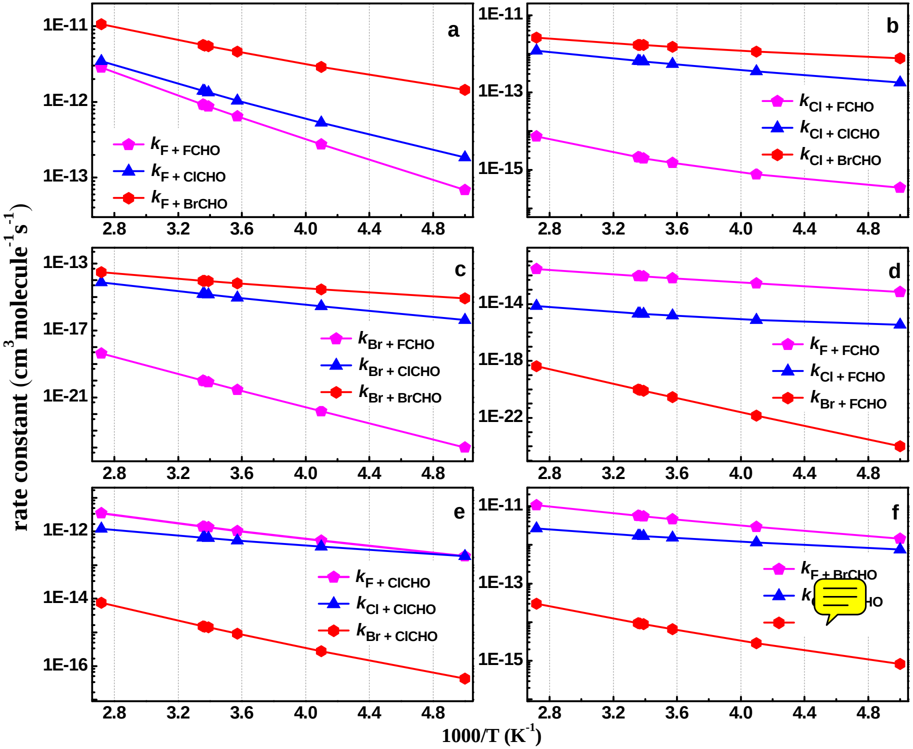

Fig. 2. ~~Plot of the CVT/SCT rate constants for the different reaction systems within the temperature range of 200–368 K.~~

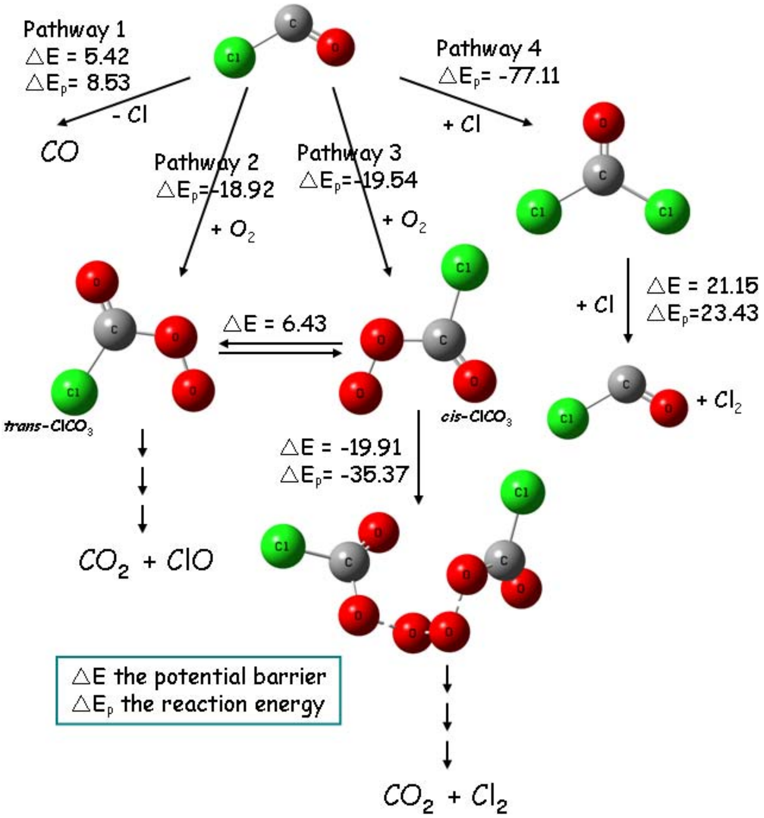

Fig. 3. Possible atmospheric degradation pathways of ClCO radical at the PMP2/6-311+G(3df,3pd)//MP2/6-311G(d,p) level (in kcal mol^{-1}).

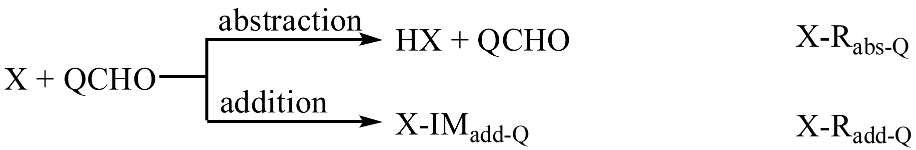

~~Fig. 1.~~ Possible pathways for the title atmospheric reactions, where QCHO represents the halogenated formaldehydes as well as Q = F, Cl, and Br. X represents the halogen atoms as well as X = F, Cl, and Br, respectively.

Supplementary Material

A theoretical model on the formation mechanism and kinetics of highly toxic air pollutants from halogenated formaldehydes reacted with halogen atoms

Y.M. Ji[1], H.H. Wang[1,2], Y.P. Gao[1,2], G.Y. Li [1], and T.C. An[1,*]

[1] State Key Laboratory of Organic Geochemistry and Guangdong Key Laboratory of Environmental Resources Utilization and Protection, Guangzhou Institute of Geochemistry, Chinese Academy of Sciences, Guangzhou 510640, China;

[2] Graduate School of Chinese Academy of Sciences, Beijing 100049, China.

Correspondence to: T.C. An (antc99@gig.ac.cn)

■ METHODS

Selection of Methods. In this work, at least 40 pathways have been calculated for the title reactions. Although the calculated time of energies for every stationary point needed for high-accuracy methods were not too long, the cumulative time for all of these stationary points were huge and not neglectable. Thus, the developments of a suitable method to balance the relationship between the computational accuracy and the computational expensive were very necessary.

In this study, the results obtained at the quadratic configuration interaction with single, double and triple excitations [QCISD(T)] methods were selected from the reference (Wu et al., 2003) (Table S1). The QCISD(T) method, a costly single-point energy (SPE) calculation method coupled with a large basis set [6-311+G(3df,2p)], could effectively minimize the error from the correlation of electrons and spin contamination effect in SPE calculation (Szabo et al., 1997). The computational results indicated that the values of PMP2//MP2 level are more closer to the values of QCISD(T) level than those of MP2//MP2 level, within the error limit of 0.47 kcal/mol. Thus, to meet the need of both high accuracy and low computational cost, the

PMP2//MP2 level was selected to carry out the calculation of the mechanisms and kinetics.

■ RESULTS AND DISCUSSION

Energies. For the pathways of F-$R_{abs\text{-}Cl}$, Cl-$R_{abs\text{-}Cl}$, F-$R_{abs\text{-}Br}$, Cl-$R_{abs\text{-}Br}$ and Br-$R_{abs\text{-}Br}$, the energy barrier heights were obtained respectively as 1.88, 1.83, 1.34, 0.94 and 3.24 kcal/mol without the ZPE corrections, but the data become negative via the ZPE correction. For testifying the negative energy barrier height, the formula $E_{a,\,298} = \Delta E_{T}^{\ddagger} + RT$ was used as a simple estimation of the activation energy (Pacey, 1981), where $\Delta E_{T}^{\ddagger} = V_{B} + \Delta ZPE + \Delta E(T)$, V_{B} and $E(T)$ represent the energy barrier height and thermal energy correction. The estimated activation energies of the pathways of F-$R_{abs\text{-}Cl}$, Cl-$R_{abs\text{-}Cl}$, F-$R_{abs\text{-}Br}$, Cl-$R_{abs\text{-}Br}$ and Br-$R_{abs\text{-}Br}$ were –2.92, –4.72, –2.78, –4.00 and –4.01 kcal/mol, respectively, which implied that all the aforementioned pathways could be nearly barrierless (Ji et al., 2008).

Rate Constants. The canonical variational transition state theory (CVT) (Truhlar et al., 1980) rate constant can be obtained by variationally minimizing the generalized transition-state theory rate constant $k^{GT}(T,s)$ with respect to the dividing surface at s, that is,

$$k^{CVT}(T) = \min_{s} k^{GT}(T,s) \qquad (1)$$

where

$$k^{GT}(T,s) = \frac{\sigma}{h\beta}\frac{Q^{GT}(t,s)}{Q^{R}(T)}\exp[-\beta V_{MEP}(s)] \qquad (2)$$

In these equations, s is the location of the generalized transition state on the intrinsic reaction coordinate (IRC); σ is the symmetry factor accounting for the possibility of two or more symmetry-related reaction paths; β equals $(k_{B}T)^{-1}$ where k_{B} is Boltzmann's constant, h is Planck's constant; $Q^{R}(T)$ is the reactant's partition function per unit volume, excluding symmetry numbers for rotation; $V_{MEP}(s)$ is the classical energy along the minimum-energy path (MEP) overall zero of energy at the reactants; $Q^{GT}(T,s)$ is the partition function of generalized transition state at s with the local zero of energy at $V_{MEP}(s)$ and with all rotational symmetry numbers set to unity. To include the tunneling effect, the CVT rate constant is multiplied by a transmission coefficient computed with the small-curvature tunneling (SCT) (Liu et al., 1993) approximation, which is denoted by k(CVT/SCT). The total rate constants for the title reactions are obtained from the sum of the individual rate constants associated.

Branching Ratio. The branching ratio Γ of each pathways was determined on the following equation, $\Gamma_n = \frac{k_n}{\sum_n k_n}$, where k_n is the reaction rate constants of *n*th pathway. In this work, the total CVT/SCT rate constants for each atmospheric reaction were obtained as the sum of the individual rate constants associated with the H-abstraction and X-addition pathways.

The Atmospheric Fate of ClCO Radical. To confirm the no barrier of these processes, the point-wise potential curve was calculated and the results is shown in Figure S7-S9. For the pathways 2 and 3, the forming C–O bonds were fixed at the values from 1.1 to 2.7 Å and from 1.2 to 3.2 Å with the interval of 0.1 Å, respectively, and the other geometric parameters were optimized for each C–O value. The minimum energy in these two pathways appeared at the C–O distance of 1.4 Å, leading to intermediates *tran*-$ClCO_3$ and *cis*-$ClCO_3$, respectively. As for the pathway 4, the forming C–Cl bond was fixed at the values from 1.3 to 4.5 Å with the interval of 0.1Å, and the other geometric parameters were optimized for each C–Cl value. The minimum energy appeared at the C–Cl distance of 1.8 Å, leading to phosgene.

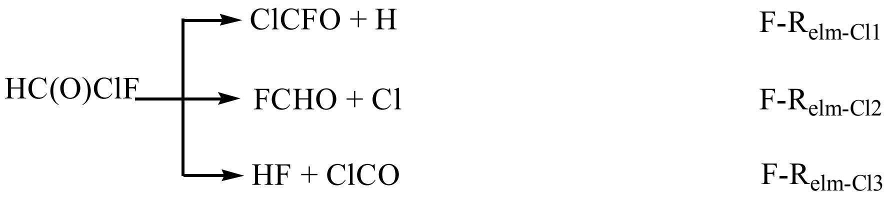

Scheme S1. For the addition intermediate HC(O)ClF, three degradation pathways: H-elimination, Cl-elimination, and HF-elimination pathways

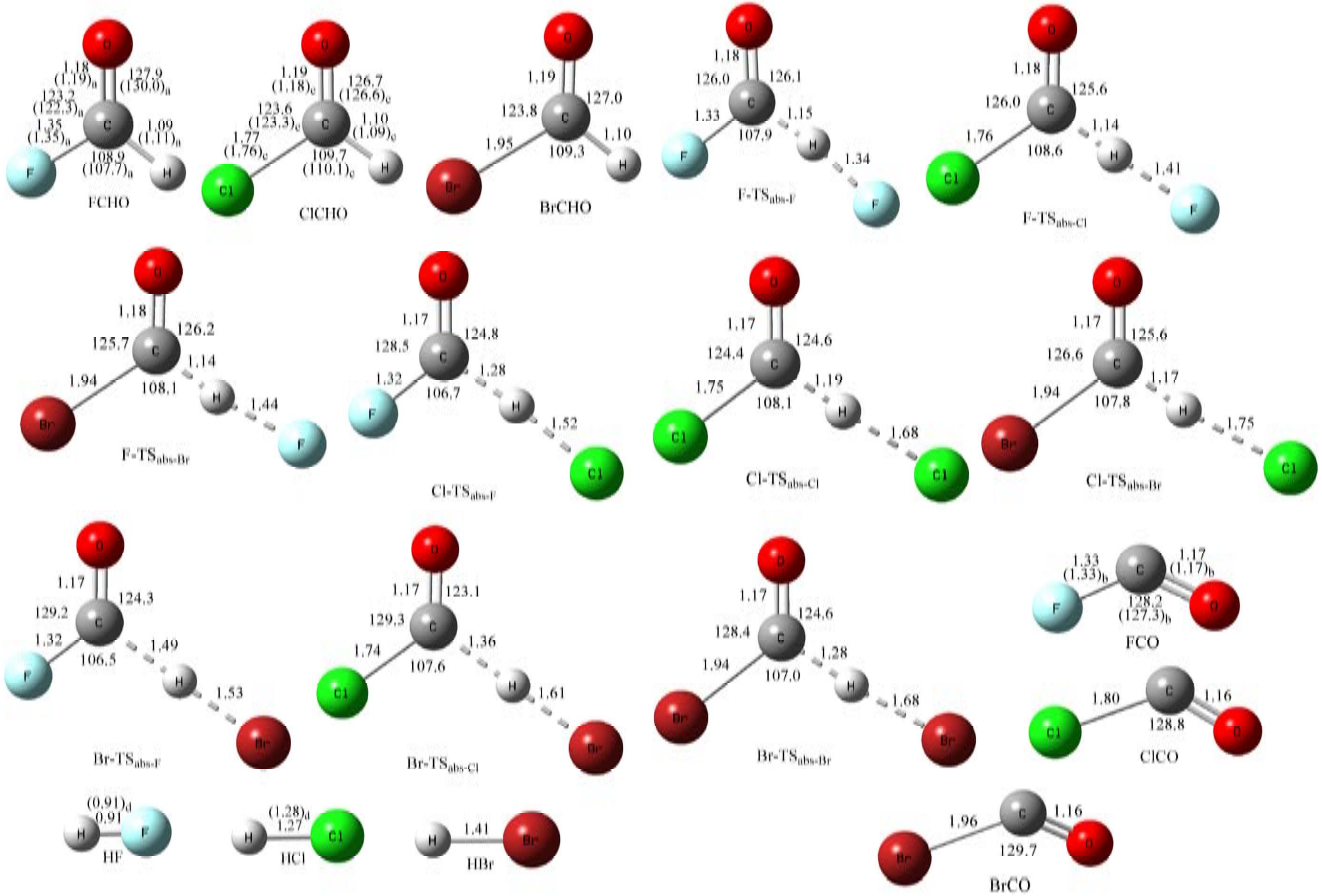

Figure S1. Optimized geometries of reactants, transition states and products involved in the H-abstraction pathways at the MP2/6-311G(d,p) level as well as the available experimental data. (Groner et al., 2001; Huisman et al., 1979; Nagai et al., 1981; NIST). (Bond lengths are in Å and angles are in °.)

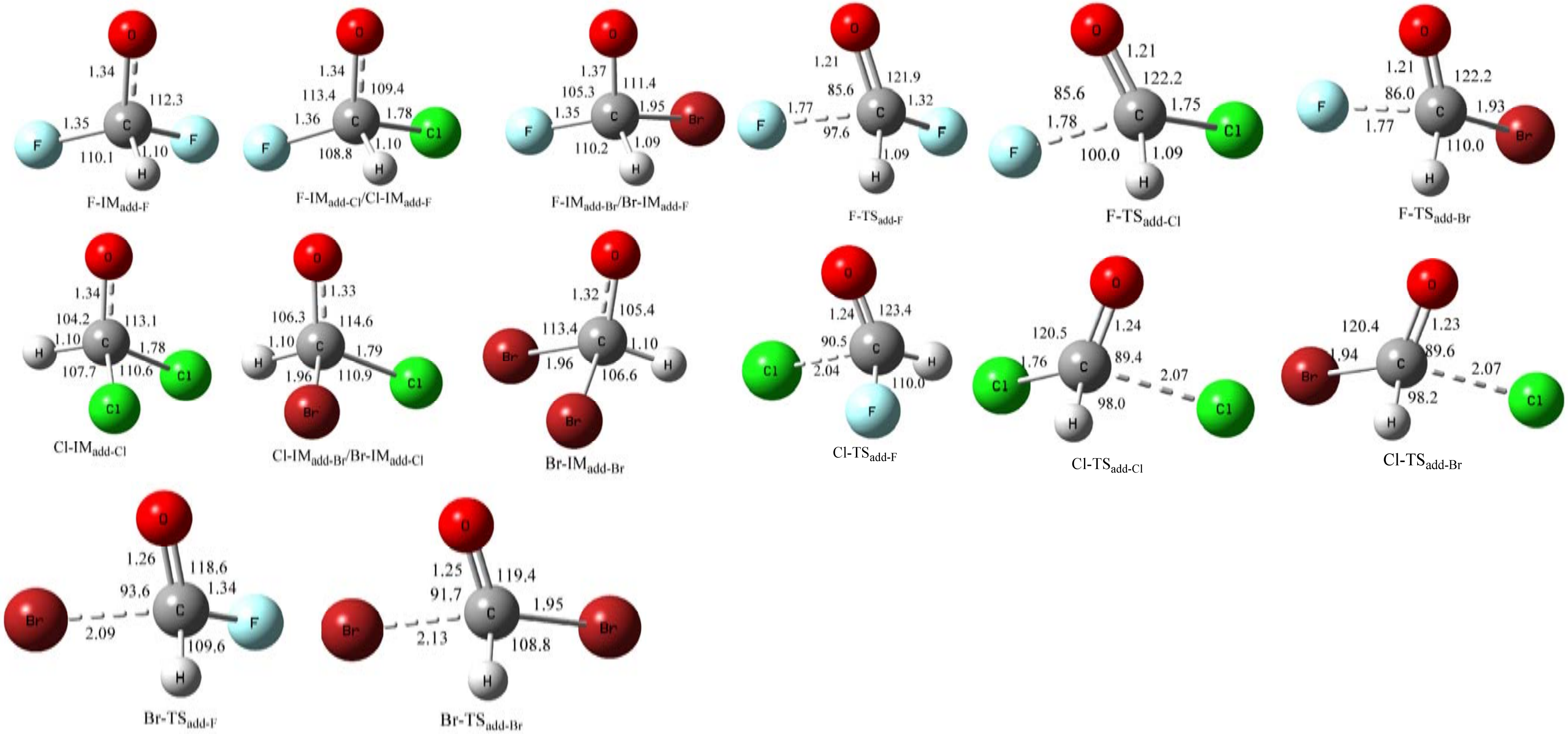

F-IM$_{\text{add-F}}$ F-IM$_{\text{add-Cl}}$/Cl-IM$_{\text{add-F}}$ F-IM$_{\text{add-Br}}$/Br-IM$_{\text{add-F}}$ F-TS$_{\text{add-F}}$ F-TS$_{\text{add-Cl}}$ F-TS$_{\text{add-Br}}$

Cl-IM$_{\text{add-Cl}}$ Cl-IM$_{\text{add-Br}}$/Br-IM$_{\text{add-Cl}}$ Br-IM$_{\text{add-Br}}$ Cl-TS$_{\text{add-F}}$ Cl-TS$_{\text{add-Cl}}$ Cl-TS$_{\text{add-Br}}$

Br-TS$_{\text{add-F}}$ Br-TS$_{\text{add-Br}}$

Figure S2. Optimized geometries of reactants, transition states, intermediates and products involved in the X-addition pathways at the MP2/6-311G(d,p) level. (Bond lengths are in Å and angles are in °.)

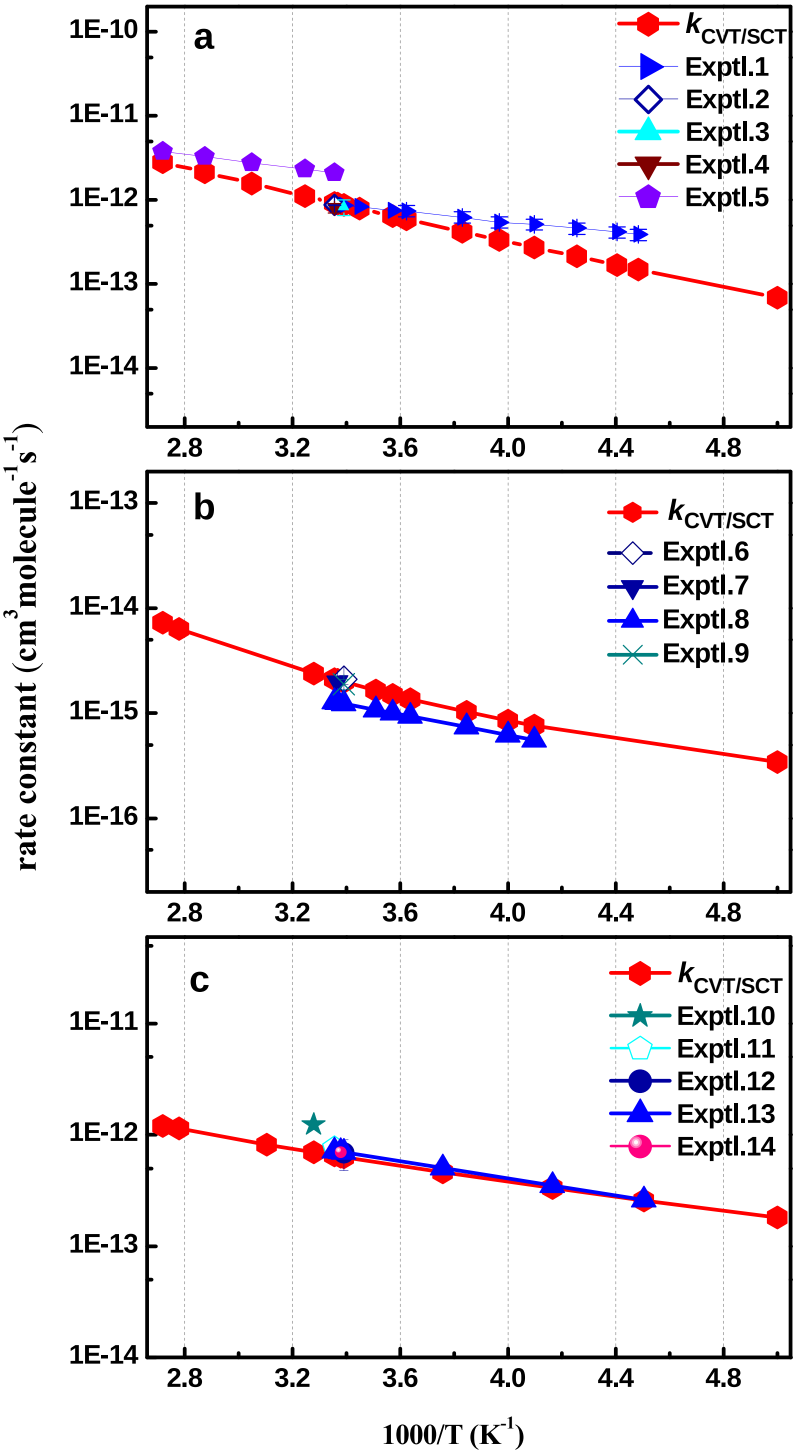

Fig. S3. Plot of the CVT/SCT rate constants calculated at the PMP2//MP2 level and the available experimental values vs 1000/T between 200–368 K for the H-abstraction pathways of (a) FCHO with F, (b) FCHO with Cl, and (c) ClCHO with Cl. Exptl. 1 from (Behr et al., 1998); Exptl. 2 from (Behr et al., 1993); Exptl. 3 from (Meagher et al., 1997); Exptl. 4 from (Hasson et al., 1998); Exptl. 5 from (Francisco et al., 1990); Exptl. 6 from (Edney et al., 1992); Exptl. 7 from (Wallington et al., 1992); Exptl. 8 from (Bednarek et al., 1996); Exptl. 9 from (Meagher et al., 1997); Exptl. 10 from (Sanhueza et al., 1975); Exptl. 11 from (Libuda et al., 1990); Exptl. 12 from (Wallington et al., 1996); Exptl. 13 from (Orlando, 1999); Exptl. 14 from (Catoire et al., 1996).

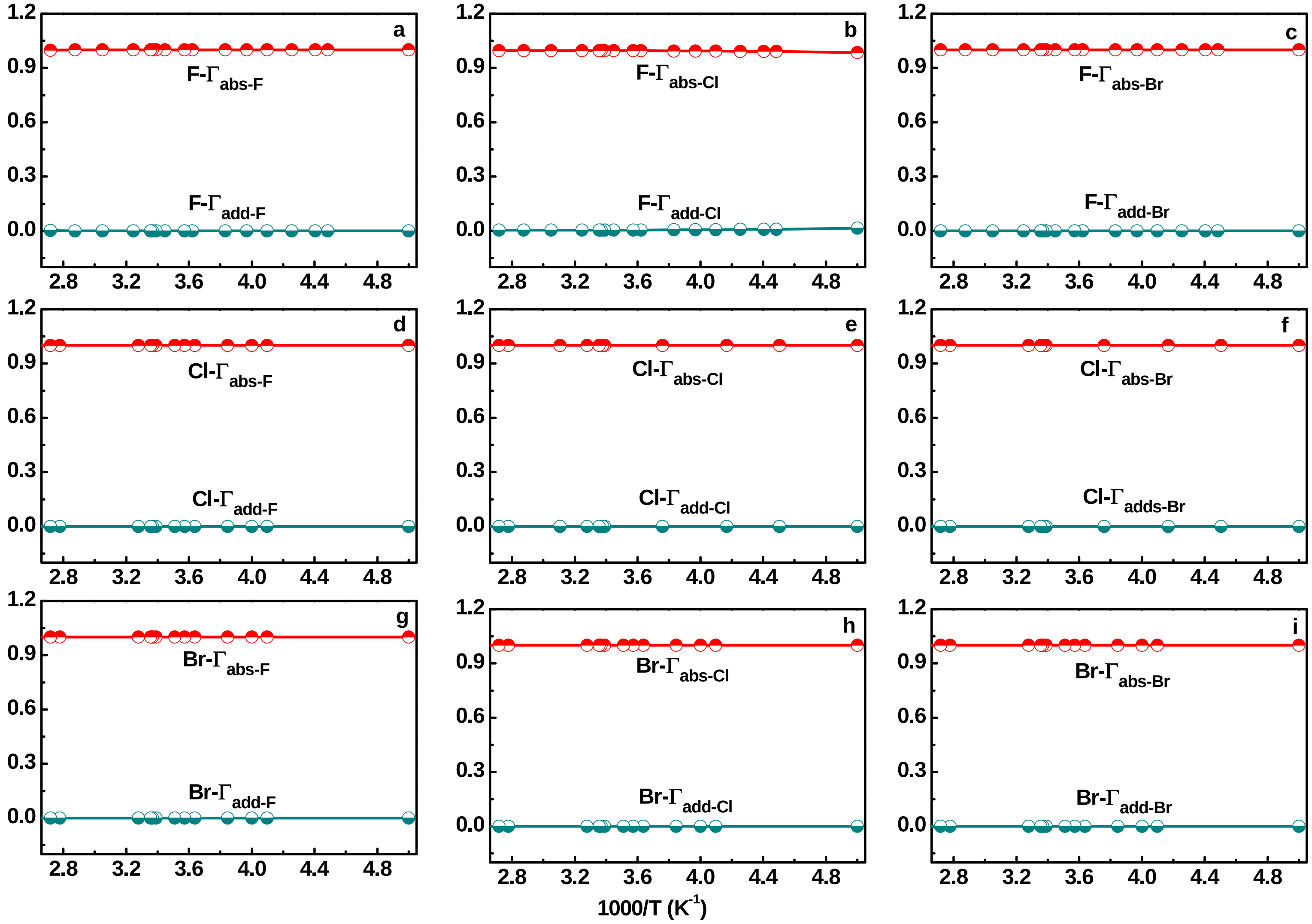

Figure S4. Plot of calculated branching ratio of the H-abstraction and X-addition pathways versus 1000/*T* between 200 and 368 K for the reactions of (a) FCHO with F, (b) ClCHO with F, (c) BrCHO with F, (d) FCHO with Cl, (e) ClCHO with Cl, (f) BrCHO with Cl, (g) FCHO with Br, (h) ClCHO with Br and (i) BrCHO with Br.

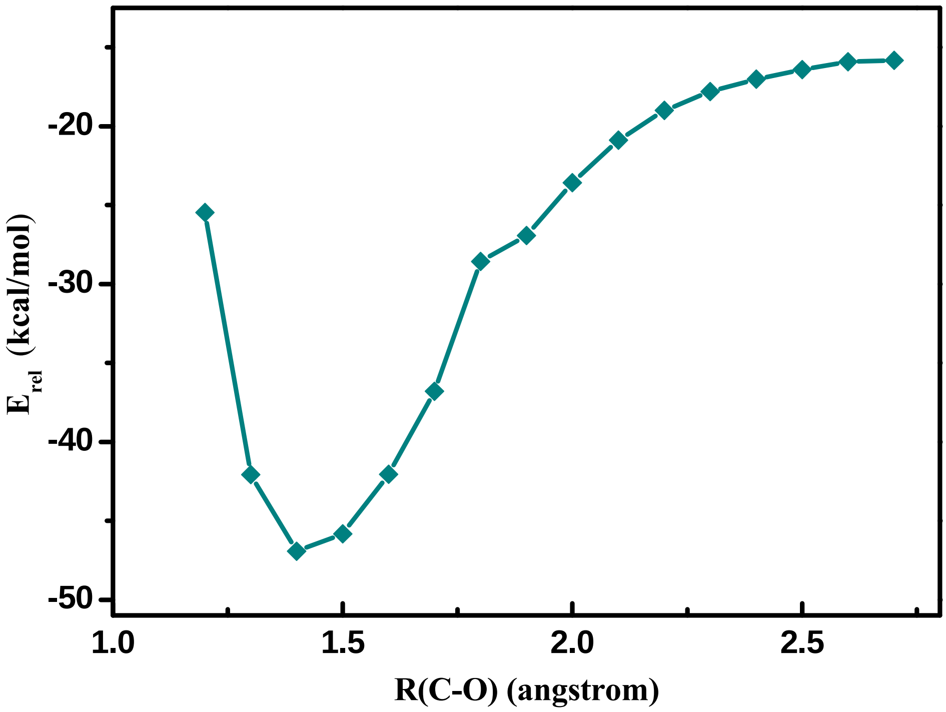

Figure S5. Potential energy curve for the formative process of *trans*-$CClO_3$ at the MP2/6-311G(d,p) level. The dotted line denotes the relative energy of ClCO + O_2.

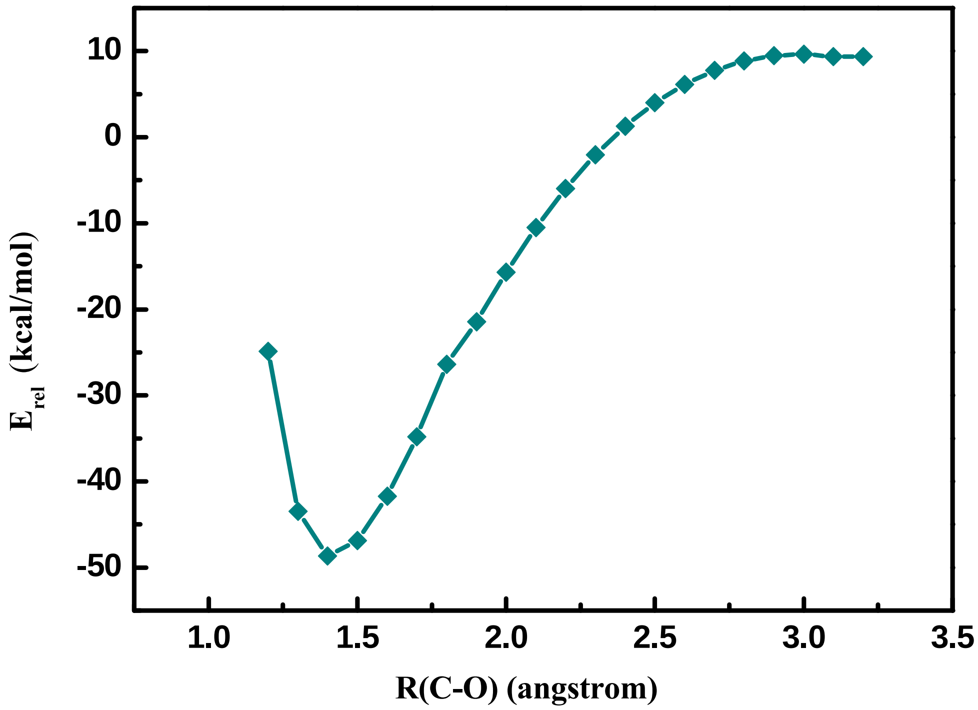

Figure S6. Potential energy curve for the formative process of *cis*-$CClO_3$ at the MP2/6-311G(d,p) level. The dotted line denotes the relative energy of ClCO + O_2.

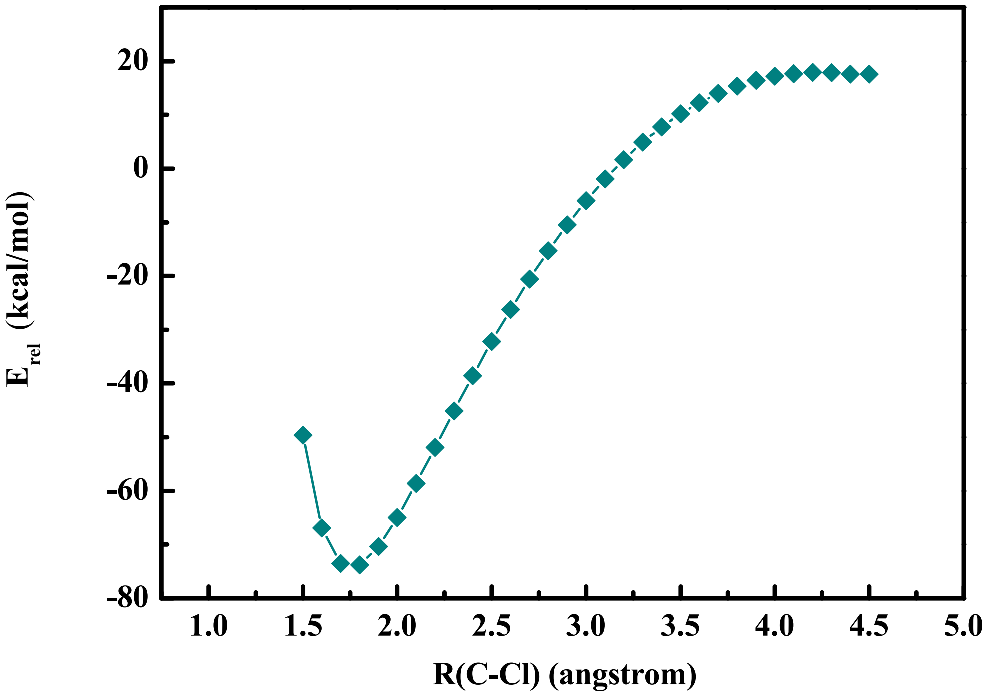

Figure S7. Potential energy curve for the formative process of phosgene at the MP2/6-311G(d,p) level. The dotted line denotes the relative energy of ClCO + Cl.

Table S1. The potential energies (ΔE) of the selected reaction pathways at the various levels. (in kcal/mol)

	[c] MP2//MP2	[d] PMP2//MP2	[e] QCISD(T)//MP2	[f] QCISD(T)//MP4	[g] MP4//MP2
[a]F-$R_{abs\text{-}F}$	3.06	1.29	1.76	1.51	2.9
[b]F-$R_{add\text{-}F}$	15.37	6.20	5.1	5.8	6.4

[a] The H-abstraction of the reaction of FCHO with F atom;

[b] The X-addition of the reaction of FCHO with F atom;

[c] The values at the MP2/6-311+G(3df,3pd)//MP2/6-311G(d,p) calculated by this work;

[d] The values at the PMP2/6-311+G(3df,3pd)//MP2/6-311G(d,p) calculated by this work;

[e] The values at the QCISD(T)/6-311+G(3df,2p)//MP2/6-311+G(d,p) calculated by Wu et al.;(Wu et al., 2003)

[f] The values at the QCISD(T)/6-311+G(3df,2p)//MP4SDQ/6-311+G(d,p) calculated by Wu et al.;(Wu et al., 2003)

[g] The values at the MP4SDQ/6-311+G(d,p)//MP2/6-311G(d,p) calculated by Franciso et al..(Francisco et al., 1990)

Table S2. Calculated frequencies of the stationary points at the MP2/6-311G(d,p) level.

species	ν	species	ν
FCHO	672, 1056, 1097, 1413, 1882, 3158	ClCHO	468, 757, 967, 1387, 1812, 3115
BrCHO	365, 656, 927, 1344, 1814, 3101	FCO	643, 1081, 1995
ClCO	375, 631, 1973	BrCO	289, 569, 1945
HF	4252	HCl	3088
HBr	2741	FCClO	421, 510, 678, 773, 1116, 1923
F_2CO	590, 626, 788, 976, 1265, 1998	FCBrO	352, 397, 635, 731, 1093, 1916
$\text{F-IM}_{\text{add-F}}$	478, 521, 656, 1007, 1153, 1176, 1362, 1414, 3093	$\text{F-IM}_{\text{add-Cl}}/\text{Cl-IM}_{\text{add-F}}$	257, 405, 589, 761, 1044, 1122, 1244, 1357, 3107
$\text{F-IM}_{\text{add-Br}}/\text{Br-IM}_{\text{add-F}}$	212, 310, 590, 600, 1030, 1137, 1171, 1389, 3141	$\text{Cl-IM}_{\text{add-Cl}}$	295, 337, 450, 695, 801, 1077, 1215, 1268, 3067
$\text{Cl-IM}_{\text{add-Br}}/\text{Br-IM}_{\text{add-Cl}}$	168, 235, 434, 592, 763, 1052, 1113, 1255, 3077	$\text{Br-IM}_{\text{add-Br}}$	174, 253, 361, 572, 683, 1078, 1099, 1208, 3057
$\text{F-TS}_{\text{abs-F}}$	1446*i*, 83, 95, 625, 861, 985, 1126, 1343, 1972	$\text{F-TS}_{\text{abs-Cl}}$	886*i*, 66, 88, 462, 731, 922, 1231, 1306, 1980
$\text{F-TS}_{\text{abs-Br}}$	732*i*, 56, 82, 365, 587, 881, 1190, 1527, 1955	$\text{Cl-TS}_{\text{abs-F}}$	1552*i*, 114, 231, 331, 704, 951, 1115, 1148, 2037
$\text{Cl-TS}_{\text{abs-Cl}}$	903*i*, 81, 194, 443, 607, 813, 935, 1246, 2035	$\text{Cl-TS}_{\text{abs-Br}}$	481*i*, 61, 171, 368, 589, 899, 1087, 1305, 1984
$\text{Br-TS}_{\text{abs-F}}$	805*i*, 98, 199, 411, 744, 769, 885, 1118, 2025	$\text{Br-TS}_{\text{abs-Cl}}$	1210*i*, 89, 222, 248, 500, 752, 861, 1045, 2071
$\text{Br-TS}_{\text{abs-Br}}$	1319*i*, 68, 211, 229, 376, 683, 863, 1104, 2039	$\text{F-TS}_{\text{add-F}}$	1199*i*, 301, 422, 688, 1071, 1165, 1425, 1641, 3202
$\text{F-TS}_{\text{add-Cl}}/\text{Cl-TS}_{\text{elm-F2}}$	1192*i*, 247, 397, 488, 800, 1033, 1404, 1567, 3162	$\text{F-TS}_{\text{add-Br}}/\text{Br-TS}_{\text{elm-F2}}$	1206*i*, 210, 359, 415, 688, 1022, 1362, 1561, 3144
$\text{Cl-TS}_{\text{add-F}}/\text{F-TS}_{\text{elm-Cl2}}$	899*i*, 282, 357, 655, 955, 1144, 1370, 1463, 3176	$\text{Cl-TS}_{\text{add-Cl}}$	888*i*, 223, 338, 467, 764, 964, 1366, 1388, 3149
$\text{Cl-TS}_{\text{add-Br}}/\text{Br-TS}_{\text{elm-Cl2}}$	893*i*, 179, 328, 371, 658, 958, 1331, 1376., 3133	$\text{Br-TS}_{\text{add-F}}/\text{F-TS}_{\text{elm-Br2}}$	605*i*, 275, 305, 633, 907, 1130, 1311, 1423, 3158
$\text{Br-TS}_{\text{add-Cl}}/\text{Cl-TS}_{\text{elm-Br2}}$	702*i*, 202, 290, 455, 737, 932, 1314, 1366, 3141	$\text{Br-TS}_{\text{add-Br}}$	714*i*, 150, 287, 358, 639, 921, 1308, 1326, 3128
$\text{F-TS}_{\text{elm-F1}}$	1776*i*, 558, 562, 778, 836, 860, 1063, 1203, 1861	$\text{F-TS}_{\text{elm-Cl1}}/\text{Cl-TS}_{\text{elm-F1}}$	1773*i*, 393, 445, 635, 696, 770, 852, 1072, 1873
$\text{F-TS}_{\text{elm-Br1}}/\text{Br-TS}_{\text{elm-F1}}$	1396*i*, 312, 359, 628, 707, 739, 821, 1054, 2281	$\text{Cl-TS}_{\text{elm-Cl1}}$	1776*i*, 292, 404, 501, 601, 607, 730, 792, 1888
$\text{Cl-TS}_{\text{elm-Br1}}/\text{Br-TS}_{\text{elm-Cl1}}$	1464*i*, 228, 331, 509, 566, 660, 712, 772, 2341	$\text{F-TS}_{\text{elm-F3}}$	702*i*, 394, 572, 718, 933, 1124, 1198, 1833, 2184
$\text{F-TS}_{\text{elm-Br3}}$	672*i*, 255, 346, 575, 644, 760, 1173, 1824, 2408	$\text{F-TS}_{\text{elm-Cl3}}$	630*i*, 324, 453, 619, 756, 859, 1176, 1734, 2339

Table S3. The imaginary frequencies and parameter L at the MP2 level. (ν in cm^{-1})

	F		Cl		Br	
	ν	L	ν	L	ν	L
FCHO	1446*i*	0.14	1552*i*	0.72	805*i*	3.50
ClCHO	886*i*	0.10	903*i*	0.22	1210*i*	1.30
BrCHO	732*i*	0.09	481*i*	0.15	1319*i*	0.67

Table S4. The enthalpies of formation ($\Delta H^{0}_{f,298}$) of the main species at PMP2//MP2 level. (in kcal/mol)

species	enthalpies	species	enthalpies
FCHO	–93.53 [a](–89.96)	FCO	–42.95 [a](–41.04)
ClCHO	–46.55	ClCO	–6.16
BrCHO	–33.46 ± 0.3	BrCO	1.78 ± 0.3

[a] Expeimental values.(NIST)

Table S5. Calculated CVT/SCT rate constants of H-abstraction and X-addition pathways of the F + QCHO reaction system. (in cm^3 molecule^{-1} s^{-1})

T(*K*)	F + FCHO → products			F + ClCHO → products			F + BrCHO → products		
	F-$k_{\text{abs-F}}$	F-$k_{\text{add-F}}$	k_{total}	F-$k_{\text{abs-Cl}}$	F-$k_{\text{add-Cl}}$	k_{total}	F-$k_{\text{abs-Br}}$	F-$k_{\text{add-Br}}$	k_{total}
200	6.84×10^{-14}	2.83×10^{-19}	6.84×10^{-14}	1.82×10^{-13}	2.57×10^{-15}	1.85×10^{-13}	1.44×10^{-12}	2.41×10^{-21}	1.44×10^{-12}
223	1.49×10^{-13}	1.46×10^{-18}	1.49×10^{-13}	3.30×10^{-13}	2.98×10^{-15}	3.33×10^{-13}	2.10×10^{-12}	2.43×10^{-20}	2.10×10^{-12}
227	1.69×10^{-13}	1.93×10^{-18}	1.69×10^{-13}	3.63×10^{-13}	3.07×10^{-15}	3.66×10^{-13}	2.24×10^{-12}	3.57×10^{-20}	2.24×10^{-12}
235	2.13×10^{-13}	3.35×10^{-18}	2.13×10^{-13}	4.36×10^{-13}	3.25×10^{-15}	4.39×10^{-13}	2.54×10^{-12}	7.53×10^{-20}	2.54×10^{-12}
244	2.74×10^{-13}	6.07×10^{-18}	2.74×10^{-13}	5.29×10^{-13}	3.48×10^{-15}	5.32×10^{-13}	2.90×10^{-12}	1.66×10^{-19}	2.90×10^{-12}
252	3.37×10^{-13}	1.00×10^{-17}	3.37×10^{-13}	6.23×10^{-13}	3.70×10^{-15}	6.27×10^{-13}	3.24×10^{-12}	3.22×10^{-19}	3.24×10^{-12}
261	4.20×10^{-13}	1.72×10^{-17}	4.20×10^{-13}	7.42×10^{-13}	3.97×10^{-15}	7.46×10^{-13}	3.66×10^{-12}	6.47×10^{-19}	3.66×10^{-12}
276	5.91×10^{-13}	3.95×10^{-17}	5.91×10^{-13}	9.74×10^{-13}	4.50×10^{-15}	9.79×10^{-13}	4.41×10^{-12}	1.89×10^{-18}	4.41×10^{-12}
280	6.44×10^{-13}	4.87×10^{-17}	6.44×10^{-13}	1.04×10^{-12}	4.66×10^{-15}	1.04×10^{-12}	4.62×10^{-12}	2.47×10^{-18}	4.62×10^{-12}
290	7.92×10^{-13}	8.05×10^{-17}	7.92×10^{-13}	1.23×10^{-12}	5.08×10^{-15}	1.24×10^{-12}	$5.18 \times 10\text{-}^{12}$	4.68×10^{-18}	5.18×10^{-12}
295	8.74×10^{-13}	1.02×10^{-16}	8.74×10^{-13}	1.33×10^{-12}	5.31×10^{-15}	1.34×10^{-12}	5.47×10^{-12}	6.35×10^{-18}	5.47×10^{-12}
297	9.08×10^{-13}	1.12×10^{-16}	9.08×10^{-13}	1.37×10^{-12}	5.41×10^{-15}	1.38×10^{-12}	5.58×10^{-12}	7.15×10^{-18}	5.58×10^{-12}
298	9.26×10^{-13}	1.18×10^{-16}	9.26×10^{-13}	1.39×10^{-12}	5.46×10^{-15}	1.40×10^{-12}	5.64×10^{-12}	7.59×10^{-18}	5.64×10^{-12}
308	1.11×10^{-12}	1.85×10^{-16}	1.11×10^{-12}	1.62×10^{-12}	5.97×10^{-15}	1.63×10^{-12}	6.26×10^{-12}	1.34×10^{-17}	6.26×10^{-12}
328	1.57×10^{-12}	4.22×10^{-16}	1.57×10^{-12}	2.13×10^{-12}	7.19×10^{-15}	2.14×10^{-12}	7.59×10^{-12}	3.80×10^{-17}	7.59×10^{-12}
348	2.14×10^{-12}	8.86×10^{-16}	2.14×10^{-12}	2.74×10^{-12}	8.70×10^{-15}	2.75×10^{-12}	9.05×10^{-12}	9.64×10^{-17}	9.05×10^{-12}
368	2.84×10^{-12}	1.73×10^{-15}	2.84×10^{-12}	3.45×10^{-12}	1.06×10^{-14}	3.46×10^{-12}	1.06×10^{-11}	2.22×10^{-16}	1.06×10^{-11}

Table S6. Calculated CVT/SCT rate constants of H-abstraction and X-addition pathways of the Cl + QCHO reaction system. (in cm^3 $molecule^{-1}$ s^{-1})

T(K)	Cl + FCHO → products			Cl + ClCHO → products			Cl + BrCHO → products		
	Cl-$k_{\text{abs-F}}$	Cl-$k_{\text{add-F}}$	k_{total}	Cl-$k_{\text{abs-Cl}}$	Cl-$k_{\text{add-Cl}}$	k_{total}	Cl-$k_{\text{abs-Br}}$	Cl-$k_{\text{add-Br}}$	k_{total}
200	3.46×10^{-16}	4.55×10^{-31}	3.46×10^{-16}	1.82×10^{-13}	3.86×10^{-38}	1.82×10^{-13}	7.58×10^{-13}	1.13×10^{-33}	7.58×10^{-13}
244	7.61×10^{-16}	7.62×10^{-28}	7.61×10^{-16}	3.51×10^{-13}	7.65×10^{-35}	3.51×10^{-13}	1.14×10^{-12}	6.62×10^{-30}	1.14×10^{-12}
250	8.50×10^{-16}	1.72×10^{-27}	8.50×10^{-16}	3.79×10^{-13}	1.79×10^{-34}	3.79×10^{-13}	1.20×10^{-12}	1.71×10^{-29}	1.20×10^{-12}
260	1.03×10^{-15}	6.14×10^{-27}	1.03×10^{-15}	4.29×10^{-13}	6.87×10^{-34}	4.29×10^{-13}	1.30×10^{-12}	7.55×10^{-29}	1.30×10^{-12}
275	1.36×10^{-15}	3.49×10^{-26}	1.36×10^{-15}	5.11×10^{-13}	4.50×10^{-33}	5.11×10^{-13}	1.46×10^{-12}	5.75×10^{-28}	1.46×10^{-12}
280	1.50×10^{-15}	5.99×10^{-26}	1.50×10^{-15}	5.40×10^{-13}	8.19×10^{-33}	5.40×10^{-13}	1.51×10^{-12}	1.08×10^{-27}	1.51×10^{-12}
285	1.65×10^{-15}	1.01×10^{-25}	1.65×10^{-15}	5.70×10^{-13}	1.47×10^{-32}	5.70×10^{-13}	1.56×10^{-12}	1.98×10^{-27}	1.56×10^{-12}
295	1.99×10^{-15}	2.71×10^{-25}	1.99×10^{-15}	6.33×10^{-13}	4.62×10^{-32}	6.33×10^{-13}	1.68×10^{-12}	6.27×10^{-27}	1.68×10^{-12}
297	2.07×10^{-15}	3.28×10^{-25}	2.07×10^{-15}	6.46×10^{-13}	5.78×10^{-32}	6.46×10^{-13}	1.70×10^{-12}	7.82×10^{-27}	1.70×10^{-12}
298	2.11×10^{-15}	3.60×10^{-25}	2.11×10^{-15}	6.52×10^{-13}	6.47×10^{-32}	6.52×10^{-13}	1.71×10^{-12}	8.73×10^{-27}	1.71×10^{-12}
305	2.40×10^{-15}	6.85×10^{-25}	2.40×10^{-15}	6.99×10^{-13}	1.41×10^{-31}	6.99×10^{-13}	1.79×10^{-12}	1.84×10^{-26}	1.79×10^{-12}
360	6.38×10^{-15}	4.55×10^{-23}	6.38×10^{-15}	1.14×10^{-12}	4.24×10^{-29}	1.14×10^{-12}	2.50×10^{-12}	2.43×10^{-24}	2.50×10^{-12}
368	7.29×10^{-15}	7.56×10^{-23}	7.29×10^{-15}	1.21×10^{-12}	9.07×10^{-29}	1.21×10^{-12}	2.62×10^{-12}	4.39×10^{-24}	2.62×10^{-12}

Table S7. Calculated CVT/SCT rate constants of H-abstraction and X-addition pathways of the Br + QCHO reaction system. (in cm^3 molecule^{-1} s^{-1})

T(*K*)	Br + FCHO → products			Br + ClCHO → products			Br + BrCHO → products		
	Br-$k_{\text{abs-F}}$	Br-$k_{\text{add-F}}$	k_{total}	Br-$k_{\text{abs-Cl}}$	Br-$k_{\text{add-Cl}}$	k_{total}	Br-$k_{\text{abs-Br}}$	Br-$k_{\text{add-Br}}$	k_{total}
200	9.93×10^{-25}	2.41×10^{-42}	9.93×10^{-25}	4.20×10^{-17}	2.48×10^{-40}	4.20×10^{-17}	8.28×10^{-16}	8.69×10^{-76}	8.28×10^{-16}
244	1.46×10^{-22}	4.82×10^{-37}	1.46×10^{-22}	2.76×10^{-16}	2.03×10^{-35}	2.76×10^{-16}	2.85×10^{-15}	1.93×10^{-64}	2.85×10^{-15}
250	2.53×10^{-22}	1.83×10^{-36}	2.53×10^{-22}	3.43×10^{-16}	6.98×10^{-35}	3.43×10^{-16}	3.31×10^{-15}	3.35×10^{-63}	3.31×10^{-15}
260	6.02×10^{-22}	1.48×10^{-35}	6.02×10^{-22}	4.86×10^{-16}	4.84×10^{-34}	4.86×10^{-16}	4.21×10^{-15}	2.92×10^{-61}	4.21×10^{-15}
275	1.98×10^{-21}	2.58×10^{-34}	1.98×10^{-21}	7.87×10^{-16}	6.82×10^{-33}	7.87×10^{-16}	5.88×10^{-15}	1.29×10^{-58}	5.88×10^{-15}
280	2.86×10^{-21}	6.24×10^{-34}	2.86×10^{-21}	9.16×10^{-16}	1.55×10^{-32}	9.16×10^{-16}	6.55×10^{-15}	8.55×10^{-58}	6.55×10^{-15}
285	4.10×10^{-21}	1.47×10^{-33}	4.10×10^{-21}	1.06×10^{-15}	3.41×10^{-32}	1.06×10^{-15}	7.26×10^{-15}	5.29×10^{-57}	7.26×10^{-15}
295	8.11×10^{-21}	7.44×10^{-33}	8.11×10^{-21}	1.41×10^{-15}	1.53×10^{-31}	1.41×10^{-15}	8.88×10^{-15}	1.68×10^{-55}	8.88×10^{-15}
297	9.25×10^{-21}	1.02×10^{-32}	9.25×10^{-21}	1.49×10^{-15}	2.05×10^{-31}	1.49×10^{-15}	9.23×10^{-15}	3.27×10^{-55}	9.23×10^{-15}
298	9.87×10^{-21}	1.19×10^{-32}	9.87×10^{-21}	1.53×10^{-15}	2.36×10^{-31}	1.53×10^{-15}	9.41×10^{-15}	4.54×10^{-55}	9.41×10^{-15}
305	1.54×10^{-20}	3.40×10^{-32}	1.54×10^{-20}	1.85×10^{-15}	6.26×10^{-31}	1.85×10^{-15}	1.07×10^{-14}	4.27×10^{-54}	1.07×10^{-14}
360	2.91×10^{-19}	3.29×10^{-29}	2.91×10^{-19}	6.54×10^{-15}	3.63×10^{-28}	6.54×10^{-15}	2.67×10^{-14}	9.39×10^{-48}	2.67×10^{-14}
368	4.17×10^{-19}	7.56×10^{-29}	4.17×10^{-19}	7.67×10^{-15}	7.84×10^{-28}	7.67×10^{-15}	3.00×10^{-14}	5.48×10^{-47}	3.00×10^{-14}

Table S8. The modified Arrhenius formulas for $k = AT^{B}\exp(-C/T)$ for H-abstraction and X-addition pathways.

pathways	*A*	B	*C*
F-R_{abs-F}	4.58×10^{-16}	1.99	1104
F-R_{add-F}	5.80×10^{-32}	7.32	1932
F-R_{abs-Cl}	6.89×10^{-17}	2.16	716
F-R_{add-Cl}	2.59×10^{-32}	6.36	-1090
F-R_{abs-Br}	3.71×10^{-16}	1.91	374
F-R_{add-Br}	1.45×10^{-25}	5.27	3659
Cl-R_{abs-F}	1.80×10^{-41}	9.78	-1274
Cl-R_{add-F}	8.68×10^{-17}	1.29	7947
Cl-R_{abs-Cl}	5.39×10^{-18}	2.20	243
Cl-R_{add-Cl}	1.45×10^{-94}	26.66	2246
Cl-R_{abs-Br}	3.50×10^{-17}	1.91	31
Cl-R_{add-Br}	7.19×10^{-16}	1.11	9376
Br-R_{abs-F}	4.21×10^{-21}	3.02	4866
Br-R_{add-F}	1.25×10^{-17}	1.68	13165
Br-R_{abs-Cl}	1.53×10^{-23}	3.96	1228
Br-R_{add-Cl}	4.74×10^{-17}	1.42	12228
Br-R_{abs-Br}	5.41×10^{-24}	4.03	501
Br-R_{add-Br}	2.39×10^{-17}	1.61	18621

Table S9. The potential barrier heights (ΔE) and reaction enthalpies (ΔH^0_{298}) for elimination pathways of the F + QCHO reaction systems (Q = F, Cl and Br). (in kcal/mol, the energy of the corresponding IM is set to be zero as reference)

	ΔE	ΔH^0_{298}
F-$R_{elm\text{-}F1}$	10.80	–5.64
F-$R_{elm\text{-}F2}$	28.75	23.73
F-$R_{elm\text{-}F3}$	28.45	–24.87
F-$R_{elm\text{-}Cl1}$	11.06	–4.97
F-$R_{elm\text{-}Cl2}$	0.76	–15.17
F-$R_{elm\text{-}Cl3}$	25.54	–33.17
F-$R_{elm\text{-}Br1}$	7.64	–7.59
F-$R_{elm\text{-}Br2}$	–9.27	–31.49
F-$R_{elm\text{-}Br3}$	20.94	–42.44

Table S10. Calculated CVT/SCT rate constants of H-abstraction and X-addition pathways at different heights[a] in the earth atmosphere. (in cm^3 molecule^{-1} s^{-1})

h (km)	*T* (K)	F + FCHO → products		F + ClCHO → products		F + BrCHO → products	
		k_{abs}	k_{add}	k_{abs}	k_{add}	k_{abs}	k_{add}
0	298.15	9.28×10^{-13}	1.19×10^{-16}	1.40×10^{-12}	5.46×10^{-15}	5.65×10^{-12}	7.66×10^{-18}
0	288.19	7.63×10^{-13}	7.37×10^{-17}	1.19×10^{-12}	5.00×10^{-15}	5.07×10^{-12}	4.18×10^{-18}
2	275.21	5.81×10^{-13}	3.79×10^{-17}	9.60×10^{-13}	4.47×10^{-15}	4.37×10^{-12}	1.79×10^{-18}
4	262.23	4.33×10^{-13}	1.85×10^{-17}	7.60×10^{-13}	4.01×10^{-15}	3.72×10^{-12}	7.10×10^{-19}
6	249.25	3.14×10^{-13}	8.47×10^{-18}	5.90×10^{-13}	3.62×10^{-15}	3.12×10^{-12}	2.57×10^{-19}
8	236.27	2.21×10^{-13}	3.65×10^{-18}	4.48×10^{-13}	3.28×10^{-15}	2.59×10^{-12}	8.45×10^{-20}
10	223.29	1.51×10^{-13}	1.49×10^{-18}	3.33×10^{-13}	2.99×10^{-15}	2.11×10^{-12}	2.50×10^{-20}
12	216.69	1.22×10^{-13}	9.27×10^{-19}	2.83×10^{-13}	2.86×10^{-15}	1.88×10^{-12}	1.29×10^{-20}
h (km)	*T* (K)	Cl + FCHO → products		Cl + ClCHO → products		Cl + BrCHO → products	
		k_{abs}	k_{add}	k_{abs}	k_{add}	k_{abs}	k_{add}
0	298.15	2.11×10^{-15}	3.65×10^{-25}	6.53×10^{-13}	6.58×10^{-32}	1.71×10^{-12}	8.88×10^{-27}
0	288.19	1.75×10^{-15}	1.39×10^{-25}	5.89×10^{-13}	2.13×10^{-32}	1.60×10^{-12}	2.88×10^{-27}
2	275.21	1.37×10^{-15}	3.57×10^{-26}	5.12×10^{-13}	4.62×10^{-33}	1.46×10^{-12}	5.90×10^{-28}
4	262.23	1.07×10^{-15}	8.04×10^{-27}	4.40×10^{-13}	9.17×10^{-34}	1.32×10^{-12}	1.04×10^{-28}
6	249.25	8.39×10^{-16}	1.56×10^{-27}	3.75×10^{-13}	1.61×10^{-34}	1.19×10^{-12}	1.52×10^{-29}
8	236.27	6.59×10^{-16}	2.52×10^{-28}	3.16×10^{-13}	2.43×10^{-35}	1.07×10^{-12}	1.82×10^{-30}
10	223.29	5.21×10^{-16}	3.31×10^{-29}	2.63×10^{-13}	3.02×10^{-36}	9.50×10^{-13}	1.70×10^{-31}
12	216.69	4.63×10^{-16}	1.08×10^{-29}	2.38×10^{-13}	9.59×10^{-37}	8.94×10^{-13}	4.57×10^{-32}
h (km)	*T* (K)	Br + FCHO → products		Br + ClCHO → products		Br + BrCHO → products	
		k_{abs}	k_{add}	k_{abs}	k_{add}	k_{abs}	k_{add}
0	298.15	9.97×10^{-21}	1.21×10^{-32}	1.54×10^{-15}	2.41×10^{-31}	9.44×10^{-15}	4.77×10^{-55}
0	288.19	5.12×10^{-21}	2.49×10^{-33}	1.16×10^{-15}	5.57×10^{-32}	7.75×10^{-15}	1.64×10^{-56}
2	275.21	2.01×10^{-21}	2.67×10^{-34}	7.92×10^{-16}	7.06×10^{-33}	5.91×10^{-15}	1.40×10^{-58}
4	262.23	7.25×10^{-22}	2.31×10^{-35}	5.23×10^{-16}	7.31×10^{-34}	4.43×10^{-15}	7.55×10^{-61}
6	249.25	2.37×10^{-22}	1.55×10^{-36}	3.34×10^{-16}	6.00×10^{-35}	3.25×10^{-15}	2.37×10^{-63}
8	236.27	6.89×10^{-23}	7.81×10^{-38}	2.06×10^{-16}	3.76×10^{-36}	2.34×10^{-15}	3.95×10^{-66}
10	223.29	1.76×10^{-23}	2.79×10^{-39}	1.22×10^{-16}	1.71×10^{-37}	1.65×10^{-15}	3.15×10^{-69}
12	216.69	8.26×10^{-24}	4.40×10^{-40}	9.15×10^{-17}	3.09×10^{-38}	1.36×10^{-15}	6.06×10^{-71}

[a] In the troposphere, the temperature drops about 6.49 K for every 1 km increase in altitude. Into the stratosphere (from 11 km height above the earth surface), the constant temperature is 216.69 K (Wikipedia, http://en.wikipedia.org/wiki/Main_Page).

REFERENCES

Bednarek, G., Breil, M., Hoffmann, A., Kohlmann, J. P., Mors, V., and Zellner, R.: Rate and mechanism of the atmospheric degradation of 1,1,1,2-tetrafluoroethane (HFC-134a), Ber. Bunsen. Phys. Chem., 100, 528-539, 1996.

Behr, P., Goldbach, K., and Heydtmann, H.: The reaction of fuorine atoms with formyl fluoride and the CFO self-reaction at 293 K, Int. J. Chem. Kinet. , 25, 957-967, 1993.

Behr, P., Kaupert, C., Shafranovski, E., and Heydtmann, H.: Temperature dependence of the gas-phase reactions F+CHFO, CFO+F, and CFO+CFO, Int J Chem Kinet, 30, 329-333, 1998.

Catoire, V., Lesclaux, R., Schneider, W. F., and Wallington, T. J.: Kinetics and mechanisms of the self-reactions of CCl_3O_2 and $CHCl_2O_2$ radicals and their reactions with HO_2, J. Phys. Chem. , 100, 14356-14371, 1996.

Edney, E. O., and Driscoll, D. J.: Chlorine initiated photooxidation studies of hydrochlorofluorocarbons (HCFCs) and hydrofluorocarbons (HFCs): Results for HCFC-22 ($CHClF_2$); HFC-41 (CH3F); HCFC-124 ($CClFHCF_3$); HFC-125 (CF_3CHF_2); HFC-134a (CF_3CH_2F); HCFC-142b ($CClF_2CH_3$); and HFC-152a (CHF_2CH_3), Int. J. Chem. Kinet. , 24, 1067-1081, 1992.

Francisco, J. S., and Zhao, Y.: The reaction of atomic fluorine with formyl fluoride: An experimental and theoretical study, J. Chem. Phys. , 93, 276-286, 1990.

Groner, P., and Warren, R. D.: Approximate r(e) structures from experimental rotational constants and ab initio force fields, J. Mol. Struct. , 599, 323-335, 2001.

Hasson, A. S., Moore, C. M., and Smith, I. W. M.: The fluorine atom initiated oxidation of CF_3CFH_2 (HFC-134a) studied by FTIR spectroscopy, Int. J. Chem. Kinet. , 30, 541-554, 1998.

Huisman, P. A. G., Klebe, K. J., Mijlhoff, F. C., and Renes, G. H.: Molecular-structure of formyl fluoride in the gas-phase as determined from electron-diffraction and microwave data, J. Mol. Struct. , 57, 71-82, 1979.

Ji, Y. M., Zhao, X. L., Liu, J. Y., Wang, Y., and Li, Z. S.: Theoretical dynamic studies on the reactions of CH3C(O)CH3-nCln (n=0-3) with the chlorine atom, J Comput Chem, 29, 809-819, 2008.

Libuda, H. G., Zabel, F., Fink, E. H., and Becker, K. H.: Formyl chloride: UV absorption cross sections and rate constants for the reactions with Cl and OH, J. Phys. Chem. , 94, 5860-5865, 1990.

Liu, Y. P., Lu, D. H., Gonzalezlafont, A., Truhlar, D. G., and Garrett, B. C.: Direct dynamics calculation of the kinetic isotope effect for an organic hydrogen-transfer reaction, including corner-cutting tunneling in 21 Dimensions, J. Am. Chem. Soc. , 115, 7806-7817, 1993.

Meagher, R. J., McIntosh, M. E., Hurley, M. D., and Wallington, T. J.: A kinetic study of the reaction of chlorine and fluorine atoms with HC(O)F at 295+/-2 K, Int J Chem Kinet, 29, 619-625, 1997.

Nagai, K., Yamada, C., Endo, Y., and Hirota, E.: Infrared diode-laser spectroscopy of FCO- the NU-1 and NU-2 bands, J. Mol. Spectrosc. , 90, 249-272, 1981.

NIST: http://webbook.nist.gov/chemistry/.

Orlando, J. J.: Temperature dependence of the rate coefficients for the reaction of chlorine atoms with chloromethanes, Int. J. Chem. Kinet. , 31, 515-524, 1999.

Pacey, P. D.: Changing Conceptions of Activation-Energy, J. Chem. Educ. , 58, 612-614, 1981.

Sanhueza, E., and Heicklen, J.: Chlorine-atom sensitized oxidation of dichloromethane and chloromethane, J. Phys. Chem. , 79, 7-11, 1975.

Szabo, A., and Ostlund, N. S.: Modern quantum chemistry, McGraw-Hill: New York, 1997.

Truhlar, D. G., and Garrett, B. C.: Variational Transition-State Theory, Acc. Chem. Res. , 13, 440-448, 1980.

Wallington, T. J., Hurley, M. D., Ball, J. C., and Kaiser, E. W.: Atmospheric chemistry of hydrofluorocarbon 134a: Fate of the alkoxy radical CF_3CFHO, Environ. Sci. Technol., 26, 1318-1324, 1992.

Wallington, T. J., Hurley, M. D., and Schneider, W. F.: Atmospheric chemistry of CH_3Cl: Mechanistic study of the reaction of CH_2ClO_2 radicals with HO_2, Chem. Phys. Lett. , 251, 164-173, 1996.

Wikipedia, http://en.wikipedia.org/wiki/Main_Page.

Wu, H. Y., Liu, J. Y., Li, Z. S., Huang, X. R., and Sun, C. C.: Theoretical study and rate constant calculation for the F+CHFO reaction, Chemical Physics Letters, 369, 504-512, 2003.